Harnessing Polyhydroxyalkanoates and Pressurised Gyration for Hard and Soft Tissue Engineering

Pooja Basnett[‡¤], Rupy K. Matharu[§¤], Caroline S. Taylor[†], Upulitha Illangakoon[§], Jonathan I. Dawson[‖], Janos M. Kanczler[‖], Mehrie Behbehani[†], Eleanor Humphrey[#], Qasim Majid[#], Barbara Lukasiewicz[‡], Rinat Nigmatullin[‡], Phoebe Heseltine[§], Richard O.C. Oreffo[‖], John W. Haycock[†], Cesare Terracciano[#], Sian E. Harding[#], Mohan Edirisinghe[§], Ipsita Roy[†#]*

[‡]School of Life Sciences, University of Westminster, London, W1W 6UW, UK
[§]Department of Mechanical Engineering, University College London, London, WC1E 7JE, UK
[†]Department of Materials Science and Engineering, University of Sheffield, Sheffield, S1 3JD, UK
[‖]Centre for Human Development, Stem Cells and Regeneration, University of Southampton, Southampton, SO17 1BJ, UK
[#]National Heart and Lung Institute, Imperial College London, London, SW3 6LY, UK

[¤]These authors have contributed equally to this work.
*Corresponding author.

KEYWORDS: *Polyhydroxyalkanoates; scaffolds; fibers; cardiac; bone; nerve.*

ABSTRACT: Organ dysfunction is a major cause of morbidity and mortality. Transplantation is typically the only definitive cure, challenged by the lack of sufficient donor organs. Tissue engineering encompasses the development of biomaterial scaffolds to support cell attachment, proliferation and differentiation, leading to tissue regeneration. For efficient clinical translation, the forming technology utilized must be suitable for mass production. Herein, uniaxial polyhydroxyalkanoate scaffolds manufactured by pressurized gyration, a hybrid scalable spinning technique, are successfully used in bone, nerve, and cardiovascular applications. Chorioallantoic membrane and *in vivo* studies provided evidence of vascularization, collagen deposition and cellular invasion for bone tissue engineering. Highly efficient axonal outgrowth was observed in dorsal root ganglion-based 3D *ex vivo* models. Human induced pluripotent stem cell derived cardiomyocytes exhibited mature cardiomyocyte phenotype with optimal calcium handling. This study confirms that engineered polyhydroxyalkanoate gyrospun fibers provide an exciting and unique toolbox for the development of scalable scaffolds for both hard and soft tissue regeneration.

1. Introduction

The lack of available organs for transplantation has motivated significant advances in tissue engineering (TE) and regenerative medicine, moving the field towards clinical application.[1] A central approach in TE is the application of 3D scaffolds for the development of functional tissue in a reproducible manner.[2,3]

A fundamental prerequisite for the ideal scaffold is the ability to mimic the natural cellular environment, creating a supportive microenvironment to stimulate cell adhesion, proliferation, differentiation and tissue morphogenesis.[4] Synthetic and natural polymers have been used to develop scaffolds, although, the former have yet to achieve the biocompatibility demonstrated by natural polymers. Synthetic polymers, such as polylactic acid, break down via bulk degradation, thus releasing acidic by-products, which can cause inflammation. In contrast, natural polymers, such as collagen, have poor yields and have variable properties.[5]

Polyhydroxyalkanoates (PHAs) are a relatively unexplored family of highly biocompatible natural polyesters that address both issues mentioned above, i.e. acidic degradation products and variable properties. The degradation products of PHAs are natural metabolites, hence non-immunogenic and hemocompatible in nature[6]; also production by highly controlled bacterial fermentation renders PHAs with highly repeatable properties. PHAs are classified into short chain length (SCL) PHAs, containing 3-5 carbon atoms within their monomeric unit, typically stiff, crystalline polymers and medium chain length (MCL) PHAs, containing 6-14 carbon atoms within their monomeric unit, typically elastomeric with a higher proportion of the amorphous phase.[7] PHAs are known for their high biocompatibility and bioresorbability, and are FDA approved for their application in bioresorbable sutures (Tepha-FLEX®).[8] The diverse monomeric composition of PHAs results in a family of materials with tunable physical properties and degradation rates. Also, PHAs exhibit degradation by surface erosion, resulting in a controlled degradation profile as opposed to bulk degradation exhibited by polylactic acid.[9] Previous unpublished work in the Roy Group indicate that PHAs are non-immunogenic and hemocompatible in nature. Given their exceptional biocompatibility, PHAs have gathered significant attention across a wide spectrum of medical applications.[9, 10]

Several fabrication technologies have been employed over the years to process bioresorbable materials into 3D scaffolds. These include solvent casting and particulate leaching (SCPL), emulsification/freeze drying, gas foaming, nanofiber self-assembly, rapid prototyping, soft lithography, three-dimensional printing, bioprinting, melt and solution electrospinning.[11, 12] Each methodology has its own merits and limitations. Amongst these, pressurized gyration is a novel, scalable processing technology used to develop 3D fibrous scaffolds.[13] It is a hybrid technique that combines centrifugal and solution blow spinning.[13] Importantly, pressurized gyration is able to produce kilograms of aligned/random fibers within an hour, independent of an electric or magnetic field, resulting in minimal production costs and the ability to process sensitive materials.[13] Electrospinning is the closest forming

technology to PG, the main advantages of the latter are the easy scalability; high production yield and the ability to spin uncharged polymers.[14, 15] Also, needle clogging is a common problem in electrospinning which reduces production yield and increases maintenance costs.[16] This may be overcome using PG. Hence, PG is a facile, cost effective, rapid and scalable technique that offers exciting opportunities in the development of multifunctional 3D fibrous scaffolds.

Here we describe the novel development of PHA based fibrous scaffolds using pressurized gyration, for hard and soft tissue engineering applications. This work introduces a step change in reproducible, rapid, economical, large scale scaffold development, essential for the successful clinical translation of tissue engineering.

2. Experimental Procedures

2.1 Production of PHAs

2.1.1. Production of SCL-PHAs, Poly(3-hydroxybutyrate) (P(3HB)): An initial seed culture was prepared by inoculating sterile nutrient broth with a single colony of *Bacillus subtilis* OK2. This was incubated for 16 hours in an orbital shaker (New Brunswick Innova 4430 Incubator Shaker, GMI Inc) at 30°C and 200 rev min^{-1}. This seed culture (10 wt% of the total production volume) was used to inoculate P(3HB) production media (modified Kannan and Rehacek media) in a sterile 15L Applikon bioreactor. Cells were cultured for 48 hours at 30°C and 200 rpm with an airflow rate of 1vvm.

2.1.2. Production of MCL-PHAs, Poly(3-hydroxyoctanoate-co-3-hydroxydecanoate) (P(3HO-co-3HD)): MCL-PHA production was carried out in two stages. An initial seed culture was prepared by inoculating sterile nutrient broth with a single colony of *Pseudomonas mendocina* CH50. This was incubated for 16 hours in an orbital shaker (New Brunswick Innova 4430 Incubator Shaker, GMI Inc) at 30°C and 200 rev min^{-1}. This seed culture (10 wt% of the total production volume) was used to inoculate the second stage seed culture (mineral salt medium). This was incubated for 16 hours in an orbital shaker (New Brunswick Innova 4430 Incubator Shaker, GMI Inc) at 30°C and 200 rev min^{-1} until the cells entered mid-log phase. The second stage seed culture (10wt% of the total production volume) was used for inoculating the final MCL-PHA production media (mineral salt media) in a sterile 15L Applikon bioreactor. Cells were cultured for 48 hours at 30°C and 200 rpm with an airflow rate of 1vvm.

2.1.3. Extraction and Purification of PHAs: Cells were recovered by centrifugation and lyophilized prior to extraction. PHAs were extracted from the dried biomass using a two stage soxhlet method.[14] Biomass was refluxed with methanol during the pre-treatment step in order to remove the impurities. The cells were then refluxed with chloroform

for 48 hours at 60°C to extract P(3HB). Chloroform solution containing PHA was concentrated using a rotary vacuum evaporator (Rotavapor R-215, Buchi). PHAs were precipitated from the concentrated chloroform solution using ice cold methanol.

2.1.4. Characterisation of PHAs: Gas Chromatography Mass Spectrometry (GC-MS) analysis was carried out to identify the monomer units of the polymer. Prior to the analysis, polymer samples were methanolysed as described in Basnett *et al*., 2020.[17] Methyl benzoate was used as the internal standard. Methanolysed samples were analysed using a Varian GC/MS system consisting Chrompack CP-3800 gas chromatograph and Saturn 200 MS/MS block.

Nuclear Magnetic Resonance (NMR) was used to identify the structure of the polymer produced. 20 mg of the polymer samples were dissolved in deuterated chloroform and analyzed using Bruker AV400 Spectrometer.

Thermal properties of the polymer were determined using Differential Scanning Calorimetry (DSC) (Perkin-Elmer Instruments, USA). Analysis of the DSC thermogram was conducted using Proteus 7.0 software.

Molecular weight of the PHAs was determined by Gel Permeation Chromatography (GPC). 2 mg/mL of polymer was introduced into the GPC system at a flow rate of 1 mL/min. The eluted polymer was detected with a refractive index detector. The data was collected and analyzed using GPC software (Aligent, Santa Clara, CA, U.S).

Mechanical properties of the PHAs were determined using a 5942 Testing Systems (Instron, High Wycombe, Buckinghamshire, U.K) equipped with 500 N load cell at room temperature. Characterization of bulk material properties was conducted using specimens of 5 mm in width and 5.0 cm in length, cut from solvent cast films. Gyrospun fibers were tested as bundles of approximately 10 mm width and 30 mm length. Before measurement, the thickness and width of the specimen were measured in several places and an average value used to calculate the cross-sectional area. The gauge length of the sample holder was set at 23 mm and a deformation rate of 5mm per minute for SCL-PHA based materials and 10 mm per minute for MCL-PHA based materials was employed. Young's modulus, tensile strength and elongation at break were calculated from the stress-strain curve and average values calculated for 3-6 specimens. Data analysis was carried out using the BlueHill 3 software (Instron, High Wycombe, Buckinghamshire, U.K).

2.2 Production of gyrospun PHA fibers

2.2.1. Preparation of Spinning Solutions: 7.4% (w/w) P(3HB) solution was prepared by dissolving P(3HB) in chloroform. In case of P(3HB)/P(3HO-*co*-3HD) blend fibers, 7.4% (w/w) P(3HB)/P(3HO-3HD) 80:20 solution was prepared by dissolving 1.92 g of P(3HB) and

0.48 g of P(3HO-co-3HD), dissolved in 30 g of chloroform. For the production of P(3HB)/HA composite fibers, 10 wt% of hydroxyapatite (HA) nanopowder (~200 nm particle size, purchased from Sigma Aldrich, U.K) was added to the 7.4 w/w% P(3HB) solution. The polymer solution was magnetically stirred for 24 hours to ensure a homogeneous dispersion.

2.2.2. Pressurized Gyration: The prepared solutions were processed into fibers using pressurized gyration. This system consists of a rotating perforated cylindrical aluminum vessel (60 mm in diameter, 30 mm in height) attached to a motor on one end and a nitrogen supply on the other (**Figure 1**). The vessel had a total of 24 perforations, each measuring approximately 0.5 mm in diameter, along the horizontal axis of the vessel. A bi-directional regulator controlled the rotating speed of the vessel. The motor could be turned on and off via a remote controller. Gas pressure can be altered with a maximum pressure of 0.3 MPa being achieved. By supplying the vessel with a constant stream of gas, jet elongation is enhanced as the polymer solution is forced through the perforations. 4 mL of the polymer solution was placed in the vessel, the vessel was sealed and spun at maximum speed with an applied pressure of 0.1 MPa.

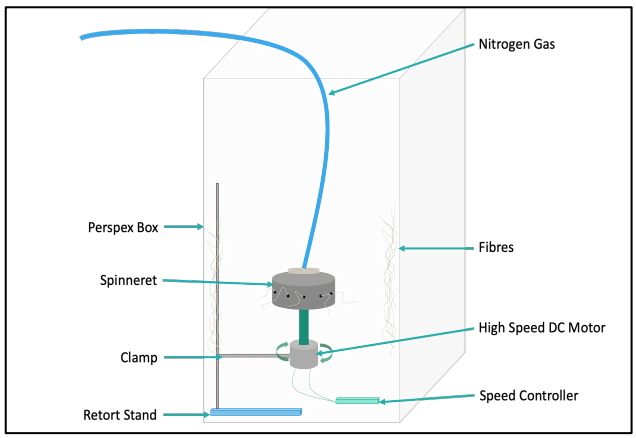

Figure 1. A schematic diagram illustrating the pressurized gyration apparatus used for fiber production

2.2.3. Characterisation of the Gyrospun Fibers: Fibers were analyzed using scanning electron microscopy (SEM) and IMAGE J software (NIH, Maryland U.S). Fibers were sputter-coated with gold (Q150R ES, Quorum Technologies) for 180 seconds prior to being imaged by SEM (Hitachi S-3400n). Using high magnification SEM images, average fiber diameter was estimated by measuring the width of approximately 100 fibers using IMAGE J. The diameter frequency distribution was modelled using OriginPro (OriginLab, Massachusetts, U.S). Average porosity was calculated by measuring the area fraction of three high magnification SEM images. Pore diameter was quantified by measuring the diameter of 50 surface pores, the longest axis was measured. Fiber alignment was estimated using OrientationJ (IMAGEJ plugin). This was achieved by calculating the directional coherence coefficient of the PHA fibers. An average of 3 measurements was taken.

2.3. Bone tissue engineering

2.3.1. Alkaline Phosphatase Assay: 1 cm^2 gyrospun fiber samples were rinsed in 100% ethanol and placed within a laminar flow cell culture hood to air dry. Samples were sterilized using UV light (250 nm) for 3 hours. Fiber samples were placed within a 24 well plate and incubated overnight in α-MEM (Minimum Essential Medium) before seeding. Stro-1+ human bone marrow stromal cells (HBMSCs) were seeded at a density of 20,000 cells per construct and cultured for 1, 7 and 21 days. Media was replaced every 2-3 days. Cell seeded samples were rinsed in cold phosphate buffered saline (PBS) and fixed in 95% ethanol for 10 minutes and rinsed in 1X PBS. 0.05% Triton X was added to the cell seeded samples and placed in a -20°C freezer for 30 minutes and thawed. The freeze/thaw process was repeated 3 times to obtain the cell lysate. 10μL of cell lysate extracted from the fiber samples was added to a 96-well plate. 90μL of substrate was added to wells with the cell lysate. Samples were incubated at 37°C between 10-60 min until samples changed color to yellow, but not as dark as the standard with the highest substrate concentration. Time taken to change color was recorded. 100μL of sodium hydroxide was added to each well (incl. standards) to terminate the reaction. The plate was read using microplate reader ELx800 (COM2) at 410 nm. Time of incubation was considered during the analyses, if incubation time was less than an hour. Alkaline phosphatase (ALP) activity was measured in nmol pNNP/mL/hr. Expression of specific activity (with respect to DNA) was measured in nmol pNPP/mgDNA.

2.3.2. Pico Green dsDNA quantitation Assay: 10μL of cell lysate (described in 2.3.1) was added into wells. 90μL TE buffer was added to the wells to make up the sample volume to 100μL. 100μL of diluted Pico Green was added to all wells. Samples were incubated at room temperature (RT), 15°C in the dark for ~5min. The plate was read in FLx800 (on COM1) spectrofluorometer at wavelengths, excitation ~480 nm; emission ~520 nm, sensitivity 90.

2.3.3. Chorioallantoic Membrane Studies (CAM studies): 1 cm^2 gyrospun fiber samples were rinsed in 100% ethanol and placed within a laminar flow cell culture hood to air dry. Samples were sterilized under the UV light (250 nm) for 3 hours. Fiber samples were placed within a 24 well plate and incubated overnight in α-MEM. Stro-1+ cells were seeded at a density of 250,000 cells per construct and cultured for 24 hours. Gyrospun fiber samples with and without cells were implanted on the extra-embryonic membrane of the developing chick for a period of 8 days as described in Moreno-Jiménez *et al*., 2016.[18] It is known that chorioallantoic membrane (CAM) starts to develop from day 4 until day 14 and it serves as the respiratory organ within the developing vascular system. Therefore, CAM studies were carried out to perform angiogenic studies as

well as to investigate the biocompatibility of the PHA based gyrospun fibers.

2.3.4 In Vivo Assessment of Bone Regeneration: 5 mm^2 gyrospun fiber samples were rinsed in 100% ethanol and placed within a laminar flow cell culture hood to air dry. Samples were sterilized under the UV light (250 nm) for 3 hours. Fiber samples were placed within 24 well plates and incubated overnight in α-MEM. Stro-1+ cells, were seeded at a density of 125,000 cells per construct and cultured for 48 hours. Gyrospun fiber samples with and without cells were co-implanted subcutaneously *in vivo* within immuno-deficient mice bilaterally along the back (3 implants separately, spaced, per group per side bilaterally; n = 3). One side received fiber implants seeded with Stro-1+ cells, while the opposite side received PHA fiber implants alone. Implants were harvested after 56 days and assessed histologically to determine the degree of bone tissue formation, angiogenesis and host tissue invasion.

2.3.5. Histology Experiments: All studies were approved by the Integrated Research Application System (IRAS project ID: 234701, protocol number: 31875, REC reference: 18/NW/0231, sponsor: University of Southampton). Prior to histology analysis, samples harvested post CAM and *in vivo* assay were dehydrated through a series of ethanol washes (50%, 90% and 100% in distilled water) and incubated with Histo-Clear solution. Samples were incubated in paraffin wax for 1 hour at 60°C and embedded in wax blocks using an automated Shandon Citadel 2000. Fine sections were rehydrated through Histo-Clear, graded ethanol and dH_2O before staining with Alcian blue/Sirius red (A/S), and Goldner's Trichrome (G/T). A/S involved staining with Weigert's haematoxylin, 0.5% Alcian blue (stains proteoglycan-rich cartilage matrix), and 1% Sirius red (stains collagenous matrix). G/T involved staining with Weigert's haematoxylin, ponceau-fuchsin-azophloxin, phosphomolybdic acid, and light green. Sections were then dehydrated and mounted with DPX before imaging on an Olympus BX-51/22 dotSlide digital virtual microscope using OlyVIA 2.1 software (Olympus Soft Imaging Solutions, GmBH, UK).

2.4. Nerve Tissue engineering

2.4.1. Live/Dead Measurement of NG108-15 Neuronal Cells and Rat Primary Schwann Cell: 24 mm^2 gyrospun fiber samples were placed in a 6 well plate. Medical grade 316 stainless rings with an internal dimeter of 13 mm were used to maintain fiber samples in position. Samples were incubated in 70% ethanol for 1 hour and rinsed twice in PBS. Fiber samples were incubated in PBS overnight prior to seeding. NG108-15 neuronal cells (ECACC 88112303) were seeded at a density of 30,000 cells per construct and rat primary Schwann cells were seeded at a density of 60,000 cells per construct. Cells were cultured on the fiber samples for 6 days. After 2 days, cell culture

medium was switched to serum free medium to initiate neurite outgrowth from NG108-15 neuronal cells. Media was replaced once on day 3. Samples were stained with 0.001% Syto-9 (Invitrogen) and 0.0015% propidium iodide (Invitrogen) at 37˚C for 30 minutes. Samples were imaged using an upright Zeiss LSM 510 confocal microscope. Three fields of view were taken, for each sample, and cells were counted using ITCN cell counter software on IMAGEJ (threshold = 40 to 90). The average number of live cells versus dead cells ± standard deviation (SD), per sample, were plotted on a graph, as well as expressed as a percentage of cell viability.

2.4.2. Neurite Outgrowth: NG108-15 neuronal cells were immunolabelled against β-III tubulin (neurite marker) and the cell nuclei were immunolabelled using 4′,6-diamidino-2-phenylindole dihydrochloride (DAPI) following the method of Behbehani *et al*. 2018.[19] Three randomly selected fields of view, for each sample, were imaged using an upright Zeiss 510 confocal microscope. Three independently run experiments were analyzed. Two parameters were used to assess NG108-15 neuronal cell differentiation: 1) the percentage of NG108-15 neuronal cells expressing neurites, and 2) the average neurite length expressed, per condition. IMAGEJ software was used to conduct cell counts and measure neurite lengths. Cell counter software (image-based tool for counting nuclei - ITCN) was used to count the number of cells per field of view, and using a 3D objects counter, cells expressing neurites were counted. This was expressed as a percentage. The ruler tool, on IMAGEJ, was used to measure the neurite length from the cell body, to the tip of the neurite, and 100 neurite lengths were examined, per condition, to calculate the average neurite length.

2.4.3. Assessment of Primary Schwann Cell Morphology: To determine the cell morphology of rat primary Schwann cells cultured onto gyrospun fibers, the average cell length was calculated as a marker. Using the ruler tool on IMAGEJ, the cell length was measured from tip to tip of the cell. For each condition, 100 primary Schwann cells were measured, and the average Schwann cell length determined for each sample ± (SD).

2.4.4. Dorsal Root Ganglion Isolation:

The methods reported in the Behbehani *et al*. 2018 [19] paper, were performed in order to determine the ability of gyrospun PHA fibers to support Schwann cell migration and neurite outgrowth from a dorsal root ganglion. Briefly, gyrospun PHA fibers were cut into bundles, and weighed, prior to being threaded into polyethylene glycol 3D printed tubes (internal diameter of 13 mm and length of 5 mm) to fill 1.9 mm^3 (40%) of the internal lumen. Chick dorsal root ganglion (DRGs) were extracted from E12 chick embryos, in compliance with UK Home Office Animals Scientific Procedures Act 1986, as previously described by Sandoval *et al*. 2020.[20] The nerve roots were trimmed and one DRG body

placed onto each sample condition and left to attach for 30 minutes. Warm supplemented DMEM, containing 10% fetal calf serum, was gently added into the well plates, and DRGs were incubated for 7 days at 37˚C/5% CO_2. The media was replaced after 3 days, and at the end of culture, DRGs were immunolabelled for β-III tubulin (neurite marker), S100β (Schwann cell marker) and the cell nuclei were immunolabelled using 4′,6-diamidino-2 phenylindoledihydrochloride (DAPI). The average neurite length of neurites outgrown from the DRG body, and the average Schwann cell migration length (100 Schwann cell lengths measured per condition), was assessed using the methods described above (neurite outgrowth method) for each condition, and experiments were conducted three times (n=3).

2.5. Cardiovascular Tissue Engineering

2.5.1. Live/Dead Measurement of Human Induced Pluripotent Stem Cell Derived Cardiomyocytes (hiPSC CMs): Gyrospun PHA fiber were sterilized in 100% ethanol for 1 hour. Fibers were allowed to air dry within a laminar flow cell-culture hood and residual ethanol was further removed by washing the fibrous scaffolds twice in sterile PBS. Sterile constructs were placed within chambers of an 8 well μ-Slide (Ibidi). hiPSC-CMs were seeded at a density of 100,000 cells per construct. Cells were allowed to adhere to the constructs for 12 hours within an incubator after which constructs were placed into fresh RPMI media containing B27 supplement. After 24-hour culture, cell seeded fiber samples were incubated with 2 μM calcein AM and 4 μM ethidium homodimer-1 solution for 30 minutes in the dark at room temperature (15°C). Samples were mounted in fresh PBS and imaged using an inverted Zeiss LSM-780 confocal microscope.

2.5.2. Sarcomere Staining: hiPSC-CMs seeded fiber samples, cultured for 7 days were rinsed in PBS, fixed with ice-cold methanol for 5 min and blocked in 1% bovine serum albumin (BSA) for an hour. Cells were stained with a primary antibody such as mouse anti- α actinin antibody (1:1000 dilution) overnight at 4°C and then incubated with a secondary antibody such as anti-mouse Cy3 antibody (1:500 dilution) for an hour at room temperature (15°C) before mounting in vecta shield (Vectalabs) mounting medium containing DAPI. The cells were imaged using an inverted Zeiss LSM-780 confocal microscope.

2.5.3. Optical Mapping- Calcium Transients of hiPSC-CMs with fluo-4 AM: Prior to recording calcium transient, the samples were placed in a sterile mattik dish and seeded with hiPSC-CMs and cultured for 7 days. They were loaded with 20 μM fluo-4 AM in DMEM and incubated for 20 minutes. Fresh DMEM was added to the samples and incubated further for 20 minutes.

2.5.4. Calcium Transients: The samples were mounted on the stage of an upright Nikon eclipse FN1 microscope in a glass bottom dish (MatTek

Corporation) and observed through a 40x water immersion objective. During the recording, cells were superfused at 37°C with Normal Tyrode's (NT) solution containing 140 mM NaCl, 4.5 mM KCl, 10 mM glucose, 10 mM HEPES, 1 mM $MgCl_2$, 1.8 mM $CaCl_2$, adjusted to pH 7.4 using 2 M NaOH. The hiPSC-CMs were field stimulated at 0.5, 1 and 1.5 Hz using an external stimulator and upon stimulation the fluorescence signal (excitation wavelength-300-520 nm and emission wavelength-480-620 nm) was recorded using a RedShirt CMOS camera (128x 128 pixels, 2 ms frame rate) and dedicated Neuroplex software (IDL, Research Systems Inc.). The fluorescence signal was then analysed using a custom MatLab code®. Four different parameters such as normalised amplitude (f_1/f_0); time to peak (T_p); time to 50% decay (T_{50}) and 90% decay (T_{90}) were assessed.

2.5.5. Statistical Analysis: Statistical analysis was performed by using GraphPad Instat (GraphPad Software, USA). One-way analysis of variance was conducted to analyse data, incorporating an unpaired T-test, ($p < 0.05$). Data is reported as means ± SD.

3. Results and Discussion

3.1. Production of PHAs: Two types of PHAs were produced via bacterial fermentation. Poly(3-hydroxybutyrate) P(3HB), a hard and stiff PHA, was produced using *Bacillus subtilis* OK2, a generally recognized as safe (GRAS) and lipopolysaccharide (LPS) free organism. Whilst poly(3-hydroxyoctanoate-co-3 hydroxydecanoate) P(3HO-*co*-3HD), a soft, ductile and elastomeric PHA was produced using *Pseudomonas mendocina* CH50 (Figure S1 and S2). The absence of LPS, a known immunogen, is a significant advantage for medical applications of the polymer.[21, 22] Both PHAs were extracted using a novel two-stage soxhlet method to ensure purity.[17] The chemical structure of the PHAs produced by microbial fermentation was established by the combination of GC-MS analysis and ^{1}H, ^{13}C NMR spectroscopy (Figures S3 – S7). The PHAs produced were of very high molecular weights exceeding 400 kDa. Both PHAs had a relatively wide molecular weight distribution with a Polydispersity Index higher than 4 (Table S1). P(3HB) and P(3HO-*co*-3HD) are semi-crystalline polymers with significant differences in melting temperatures and glass transition temperatures (Figure 7). The glass transition temperatures at -42 and 3 °C for P(3HO-co-3HD) and P(3HB) respectively means the amorphous phase of both the PHAs is in a rubbery state in physiological conditions. Melting temperatures, 57 and 171 °C for P(3HO-*co*-3HD) and P(3HB) respectively, are higher than body temperature which is necessary for the mechanical stability of the material under physiological conditions.

The mechanical properties of PHAs were characterized using tensile testing (**Figure 2, Table 1**). The stress-strain curves demonstrated the

difference in mechanical properties between the two PHAs. P(3HB) exhibited significantly higher ultimate tensile strength and lower elongation at break in comparison to P(3HO-*co*-3HD). The P(3HB) homopolymer belongs to the family of SCL- PHAs, which in general are known as stiffer and stronger materials. Whereas, P(3HO-*co*-3HD), is a MCL-PHA copolymer, which is known to demonstrate more elastomeric mechanical properties.[23] Mechanical properties of PHA-based materials can be modified by blending PHAs or filling with inorganic particles including biologically active fillers such as HA. Thus, blending of P(3HB) with 20 wt.% of P(3HO-co-3HD) allowed softening of the biomaterial and decreased the Young's modulus from 1300 to 920 MPa. This was accompanied with an almost ten-fold increase in the material's elongation at break. On the other hand, filling P(3HB) with 10 wt.% of HA resulted in an increase of Young's modulus from 1300 to 2500 MPa. However, the P(3HB)/HA composite withstood only very small deformations, around 1% compared with 3.6% for the neat polymer. The results for these four materials demonstrate that mechanical properties of PHA-based materials can be adjusted for a specific application, i.e., for soft or hard tissue engineering.

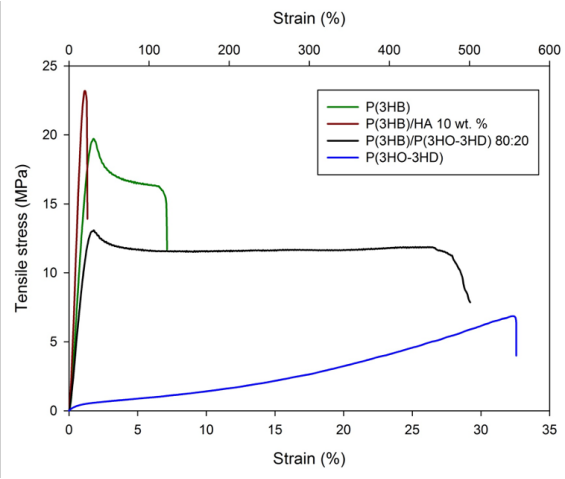

Figure 2: Representative stress-strain curves of P(3HB), P(3HO-*co*-3HD), P(3HB)/P(3HO-co-3HD) 80:20, and P(3HB)/HA composite obtained using solvent cast films.

Table 1. Mechanical properties (ultimate tensile strength (σ_U), Young modulus (E), and elongation at break (ε)) of the bulk materials.

	σ_U, MPa	E, MPa	ε, %
P(3HO-*co*-3HD)	10.4±0.5	8.7±0.8	580±40
P(3HB)	26±2	1300±150	3.6±1.1
P(3HB)/P(3HO-*co*-3HD) 80:20	12±0.8	920±100	30±5
P(3HB)/HA	21±3	2500±300	1.17±0.06

P(3HB) has been explored extensively for bone related applications whereas elastomeric PHAs such as P(3HO-*co*-3HD), have been investigated extensively for soft tissue engineering applications.[24] In this study, we have used these PHAs to create multifunctional 3D fibrous scaffolds for bone, nerve and cardiac tissue engineering.

3.2. Gyrospun PHA Fibers: Gyrospun P(3HB), P(3HB)/P(3HO-*co*-3HD) blend and P(3HB)/HA composite fibers were produced. Aligned and random fibers were found to be porous and cylindrical in shape (**Figure 3**). A coherence coefficient close to 1 indicated a strongly coherent orientation of the local fibers, i.e. aligned/uniaxial fibers.[25] The average coherence coefficient for aligned P(3HB) fibers was 0.564, for the aligned P(3HB)/P(3HO-*co*-3HD) blend fibers was 0.272 and for the aligned P(3HB)/HA composite fibers was 0.405. The average fiber diameter of the P(3HB), P(3HB)/P(3HO-*co*-3HD) blend and P(3HB)/HA composite fibers were found to be 6.9±1.9 μm, 9.1±3.7 μm and 2.5 ±0.7 μm respectively, with the blend fibers exhibiting the largest diameter. Addition of P(3HO-*co*-3HD), an elastomeric PHA with adhesive like properties to P(3HB), decreased the polymer chain overlap and entanglement and therefore decreased the viscosity and surface tension of the spinning-solution to below the critical viscosity for pressurized gyration. Therefore, the spinning solution did not have sufficient resistance to overcome the centrifugal force and formed thin fibers.

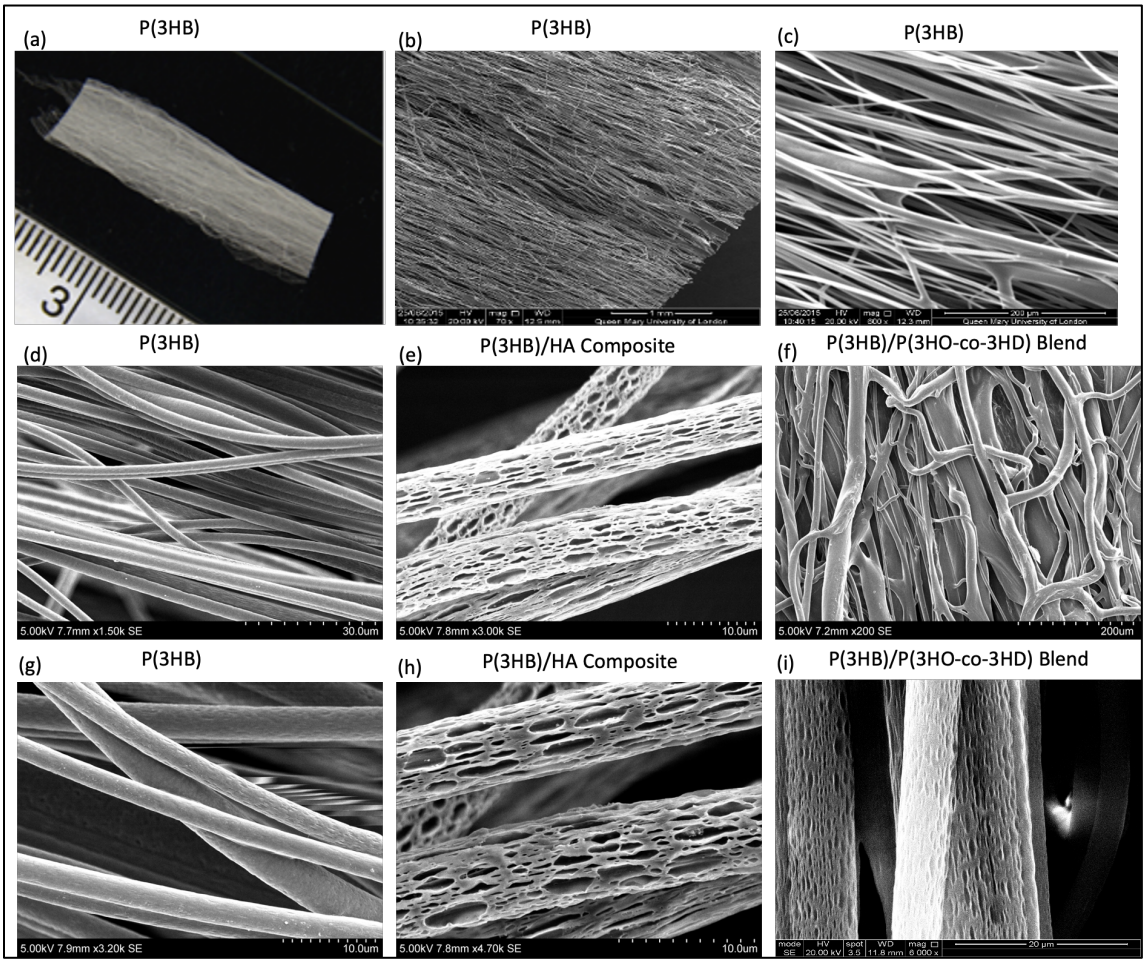

Figure 3: (a) Optical image of the gyrospun P(3HB) fibrous sheet; (b) and (c) Low resolution SEM images of the P(3HB) fibrous sheet showing the morphology and alignment of the fibers in the scaffolds; (d) and (g) High resolution SEM images of the P(3HB) fibers within the scaffolds; (e) and (h) P(3HB)/HA composite fibers illustrating the uniform distribution of 200 nm hydroxyapatite particles and the high porosity of the scaffolds; (f) P(3HB)/P(3HO-*co*-3HD) 80:20 random blend fibers and (i) P(3HB)/P(3HO-*co*-3HD) 80:20 aligned blend fibers within the gyrospun scaffolds.

The darker shades on the fibers (as seen in the SEM images in Figure 3) indicate the presence of surface pores. All fabricated fibers exhibited surface porosity, with average pore diameters of 0.52 $\pm 0.18 \mu$m, 3.97 $\pm 1.49 \mu$m and 1.09 $\pm 1.33 \mu$m being achieved in the P(3HB), P(3HB)/P(3HO-*co*-3HD) blend and P(3HB)/HA composite fibers, respectively, an essential feature of an ideal scaffold, facilitating cell adhesion, nutrient and oxygen transfer. The porosity of the P(3HB), P(3HB)/P(3HO-*co*-3HD) blend and P(3HB)/HA composite fibers were measured to be 31.0±3.2, 33.0±1.7 and 24.5±1.7μm respectively. The formation of surface pores occurred by a combination of the breath figures phenomenon, a complex process dependent upon polymer concentration, solvent volatility, phase separation, amongst others.[26] During the gyration process, evaporative cooling of chloroform resulted in the temperature at the air-liquid interface to decrease rapidly, due to the enthalpy of vaporization. This temperature drop significantly lowered the dew point of the atmosphere and led to moisture nucleation and the deposition of small water droplets onto the polymer surface. A stable polymer/water interface prevented coalescence.[27] The water droplets would have then increased in size and immersed into the polymer solution owing to the Marangoni convection and thermocapillary effects.[28-30] As the chloroform is immiscible with water, this would limit the penetration of the water droplets to the fiber core. The water droplets self-arranged into an ordered array on the solution surface and evaporation of the solvent and water droplets left pores on the surface of the formed fiber.[31] The light grey features were premature pores that were not fully developed, thus giving each fiber a nanotopography, also known to promote cell adhesion, interaction and transmigration.

Bundles of gyrospun fibers of P(3HB) and its composite with HA were characterized using tensile testing **(Figure 4).** The fibrous materials exhibited increased deformability with elongation at break of 5 and 14% for P(3HB) and its composite respectively. This is probably due to straightening and alignment of fibers in the bundles.

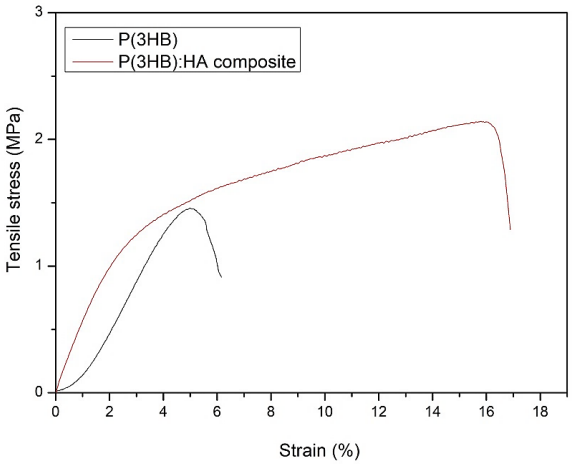

Figure 4: Representative stress-strain curves of bundles of gyrospun P(3HB) fibers and P(3HB) composite fibers.

The observed values of Young's modulus were 34 and 64 MPa for P(3HB) and its composite fibers, which are 38 and 39 times lower respectively than the corresponding bulk materials, as detailed in Table 1. A similar decrease in stiffness has been observed for electrospun fiber scaffolds as compared to the bulk material. For example in Munj *et al*., 2017, the Young's modulus of electrospun scaffolds produced using PMMA and PCL were 9.0 and 15.3 MPa, as opposed to the bulk material properties of 2800 ±70 and 354 ±10 MPa respectively.[32-34] We can hence conclude that generation of fibrous scaffolds leads to a sharp decrease in the apparent Young's modulus of the scaffold as compared to the bulk properties of the material. This explains how in this work, an inherently stiff material, P(3HB), has been successfully used to support soft tissue growth, i.e., nerve and cardiac tissue in the form of gyrospun fibers, yet another advantage of fibrous scaffolds. It is known that the scaffold architecture (fiber size, alignment and morphology) has an impact on cell behavior and function.[35-37] Based on the particular tissue engineering application, specific fiber diameter/morphology is desired. For instance, in skin tissue engineering applications, where the scaffold was required to mimic the extracellular matrix, nanofibers facilitated tissue formation.[38] In the case of nerve tissue engineering, a direct correlation was observed between the electrospun polycaprolactone fiber diameter, neurite outgrowth and Schwann cell morphology.[38] When studying neuronal cells alone, the longest neurites were observed on the large fiber diameters (~8μm). However, when studying neuronal cells and glial co-cultures, 1μm fibers supported superior neurite outgrowth and Schwan cell migration.[19, 39] In addition to fiber diameter, fiber alignment has been reported to affect the cell phenotype and function, through the provision of guidance cues to cells. This is true for several cell lines including neuronal, cardiovascular, skeletal, endothelial and fibroblast cell lines.[41-44] Fiber alignment has been shown to influence a change in the phenotype in human dermal fibroblasts with elongation along the aligned fiber.[41] Apart from effects on the cell phenotype, fiber alignment is also known to direct the deposition of collagen, secreted from the human dermal fibroblasts (HDF).[43]

Fiber alignment and diameter is also vital in peripheral nerve repair for promoting Schwann cell elongation, direction and providing a guidance

cue for the regenerating axon.[19] Furthermore, alignment is known to be crucial for cardiovascular tissue engineering with cardiomyocyte alignment enabling synchronous cell contractions, a prerequisite for effective cardiac function.[42]

3.3 Bone Tissue Engineering: Complex bone fractures and fractures that progress to non-union, coupled with co-morbidities emphasize the need for bone regeneration strategies. Although autologous bone grafting is still considered to be the gold standard, recent research has focused on the use of biomaterials to elicit healing in bone defects.[45] In the context of bone TE, properties of aligned P(3HB) and P(3HB)/HA composite fibers combined with human bone marrow stromal cells (HBMSCs) were studied, including enriched skeletal stem cell populations for bone regeneration. The *in vitro* response of the gyrospun PHA fibers in terms of cell viability, differentiation and mineralization was studied (**Figures S8 - S11**). Cell viability measured by quantification of double stranded (ds) DNA present on the gyrospun fibers, indicated increased DNA content with time, an evidence of cell attachment and proliferation on the fibers (**Figure S10**).[46-49]

Cell differentiation was assessed by quantification of alkaline phosphatase expression (**Figure S8**), a marker for early osteogenic differentiation.[50] ALP expression is associated with the elevation of the local concentration of inorganic phosphate, central to bone mineralization. Alkaline phosphatase expression was significantly higher following the culture of the Stro-1+ HBMSCs in osteogenic media over 21 days. In addition, EDX analysis qualitatively confirmed HA deposition on the gyrospun PHA fibers, following incubation in simulated body fluid (SBF) for 21 days (**Figure S11**). Formation of the hydroxyapatite crystals on the surface of an implant correlated with the *in vivo* bone bioactivity.[51, 52] Thus, P(3HB) and P(3HB)/HA composite fibers demonstrated excellent potential as scaffolds to support and enhance bone formation.

3.3.1. Evaluation of the Osteoinductive Properties of the Gyrospun PHA Fibers on the Chorioallantoic Membrane (CAM) In Vivo Model: The advantages of the chorioallantoic membrane for analysis of the gyrospun PHA fibers resides in the comparative ease of access, the under-developed immunocompetent system, rapid vascular development of the CAM and the relative low costs of running this less sentient *in vivo* model. The fibrous scaffolds were seeded with Stro-1+ cells and placed on the CAM of the chick embryos for 8 days of incubation, followed by histological analysis (**Figure 5**). The CAM implanted fibers were processed for tissue histochemistry using Goldner's Trichrome (G/T) staining.

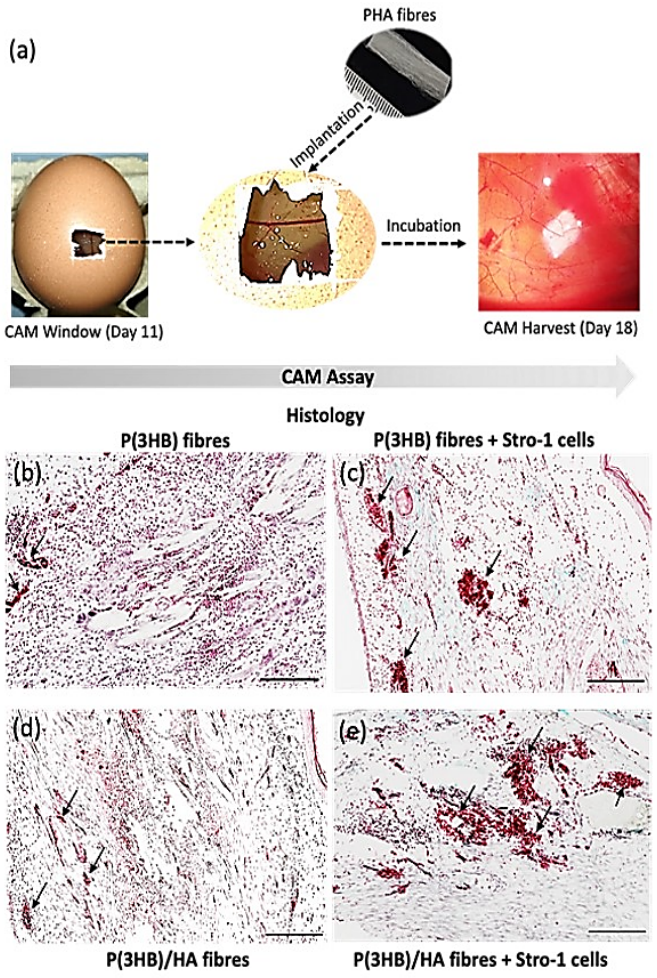

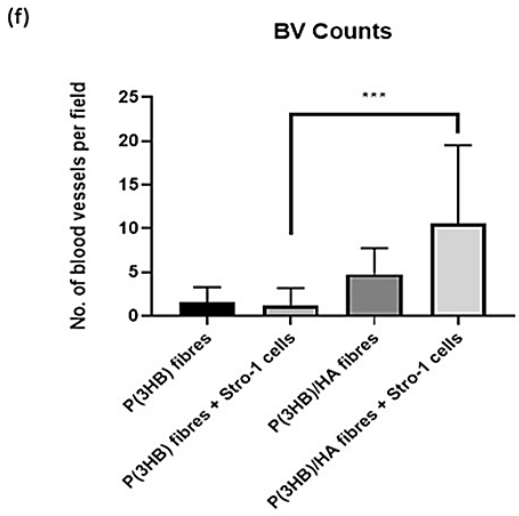

Figure 5: (a) CAM implantation: P(3HB) and P(3HB)/HA gyrospun fibers seeded with and without Stro-1 cells were implanted on the CAM of the chick embryo for 7 days after which they were harvested. Histological sections of (b) P(3HB) fibers, (c) P(3HB)/HA composite fibers, (d) P(3HB) fibers and (e) P(3HB)/HA seeded with Stro-1 cells implanted on CAM and stained with G/T (scale bar = 200 µm), (f) graph showing the number of blood vessels identified on the scaffolds using CellProfiler image analysis software after 7 days of incubation.

At the end of the implantation period, the chick embryo survival rate was 100%. P(3HB) and P(3HB)/HA composite fibers were unaltered following CAM culture. The presence of erythrocytes was marked by positive G/T stain. Erythrocytes (Figure 5(b)(c)(d)(e)- stained bright red indicated by arrows) were observed in both P(3HB) and P(3HB)/HA composite fibers confirming vascularisation, pivotal in bone remodelling.[53] The histological data related to the CAM control with no scaffold is shown in the **Figure S16**. In comparison to the other fiber implants (an average of 1.56 ±1.74 blood vessels identified on P(3HB) samples), P(3HB)/HA composite fiber implants with Stro-1+ cells displayed the highest level of vascularisation (an average of 10.6 ±8.95 blood vessels were identified).[53] The increased number of blood vessels in scaffolds seeded with Stro-1+ populations is consistent with the well-established paracrine influence of bone marrow stromal cells on vascularization [54, 55]. Though not significant, an increase in vessel number was also apparent in P(3HB)/HA composite implants, possibly due to increased porosity. The CAM study confirmed the potential of the PHA gyrospun

fibers to host angiogenesis and thus show promise as bioactive scaffolds for bone regeneration.

3.3.2. In Vivo Assessment of Bone Regeneration in Gyrospun PHA Fibers Seeded With/Without Bone Marrow Derived Stro-1+ Cells: Gyrospun PHA fiber segments were co-implanted subcutaneously *in vivo* within immuno-deficient mice as described in section 2.3.4. Explants were assessed histologically to determine the degree of bone tissue formation, angiogenesis and host tissue invasion (**Figure 6, Figure S12**).

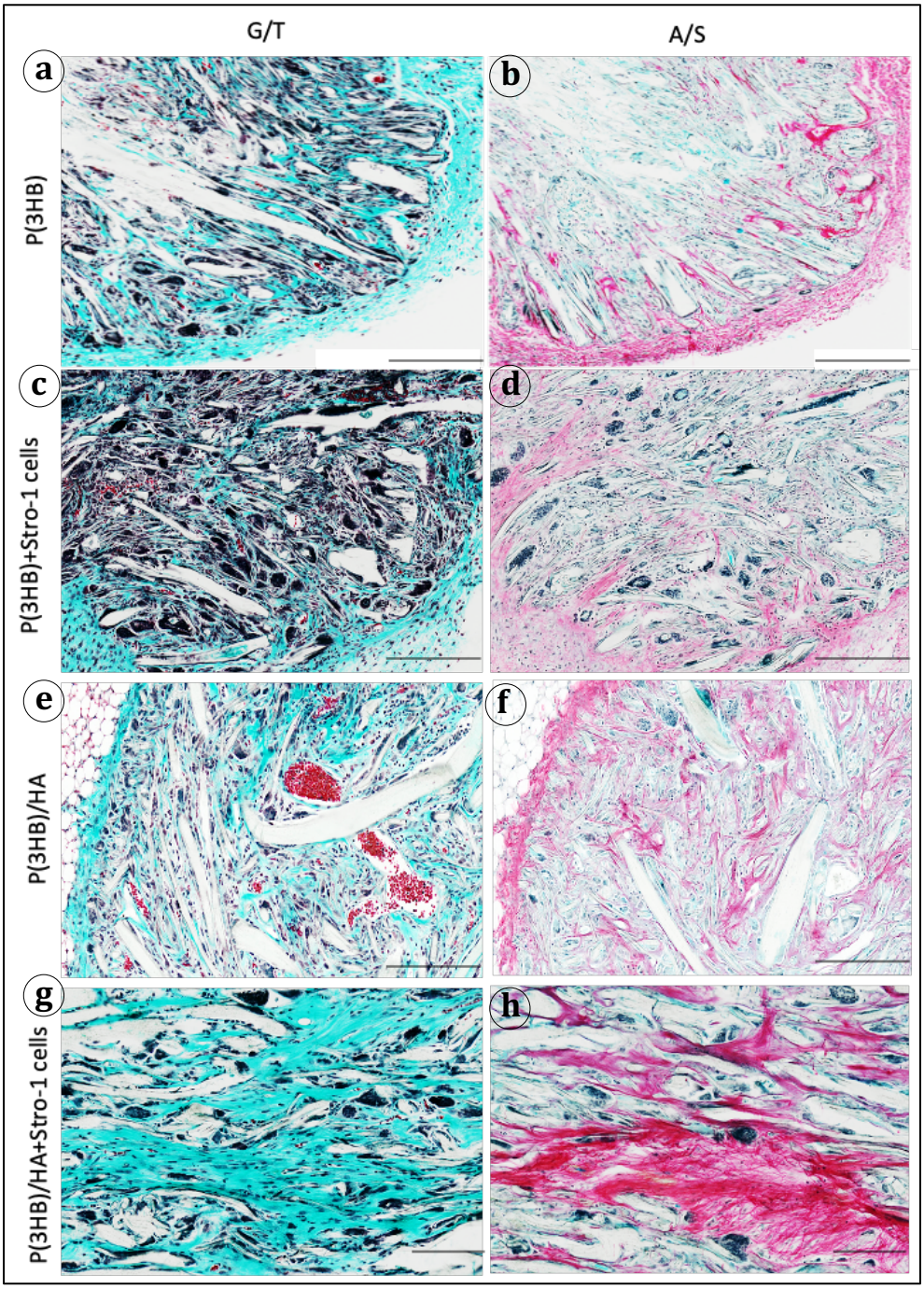

Figure 6: Histological analysis of the gyrospun (a) P(3HB) fibers stained with Goldner's Trichrome (G/T) and (b) Alcian blue/Sirius red (A/S) stain (c) P(3HB) fibers + Stro-1 cells stained with Goldner's Trichrome (G/T) and (d) Alcian blue/Sirius red (A/S) stain, (e) P(HB)/HA fibers stained with Goldner's Trichrome (G/T) and (f) Alcian blue/Sirius red (A/S) stain, (g) P(3HB)/HA fibers + Stro-1 cells stained with Goldner's Trichrome (G/T) and (h) Alcian blue/Sirius red (A/S) stain (scale bar = 200μm)

The presence of collagenous protein throughout the gyrospun PHA fiber network was evidenced by the extensive Sirius red staining and G/T staining. P(3HB)/HA composite fiber implants containing HBMSC enriched Stro-1 cells exhibited greater collagen deposition compared to the other PHA fiber implants without cells and small regions of ectopic bone formation was apparent on the P(3HB)/HA composite fiber implants containing HBMSC enriched Stro-1 cells **(Figure 7)**.[53] The presence of erythrocytes (stained bright red with G/T staining) confirmed vascularisation of the gyrospun PHA fibers by the host tissue with P(3HB)/HA composite fiber implants displaying the highest level of vascularisation (**Figure 6f, 6h**).[53,56] These results highlight the significant promise of the PHA gyrospun fibers for bone TE, without the need of additional external growth factors such as the bone morphogenic proteins.

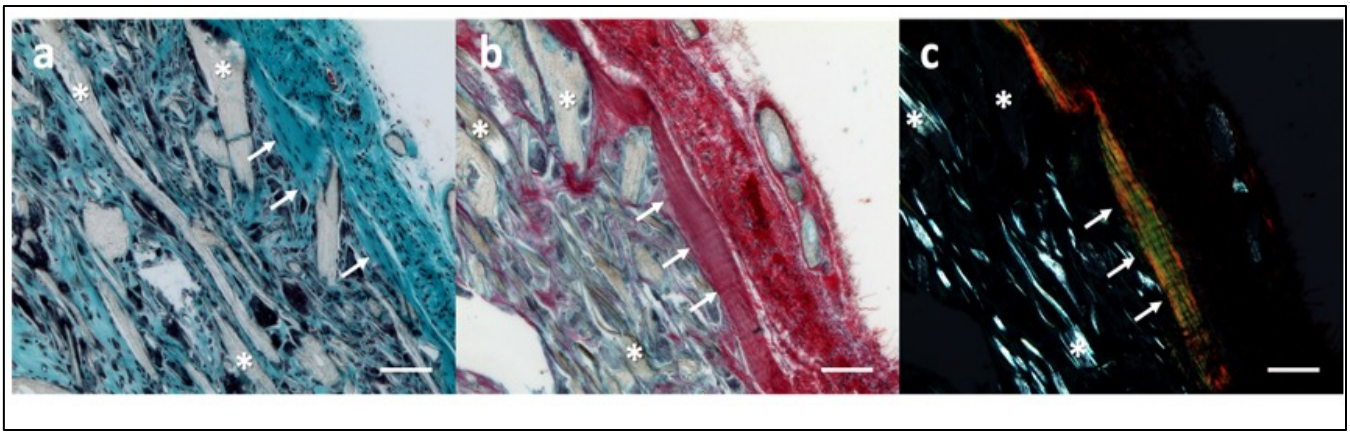

Figure 7: Ectopic bone formation by Stro-1+ HBMSC cells on implanted P(3HB)/HA fibres. Goldners' trichrome (**a**) and Sirius red staining (**b**) revealed osteoid-like collagen matrix (white arrows) around the periphery of Stro-1+ cell seeded P(3HB)/HA fibres (fibres indicated with a *). Polarised light microscopy shows collagen fibre organisation (**c**). Scale bar = 100 μm.

3.4. Nerve tissue engineering: Peripheral nerves have the ability to regenerate when injuries present a gap of less than 5mm to bridge. For larger gaps, several nerve guidance devices are being explored, however, regeneration distance is limited (typically 20-25mm in humans, and 10-15 mm in rat sciatic nerve models).[57] We investigated the properties of aligned P(3HB) and P(3HB)/P(3HO-*co*-3HD) blend gyrospun fibers as intraluminal fiber scaffolds for nerve guidance devices, for enhancing regenerative properties. The *in vitro* response to PHA fibers in terms of cell viability, differentiation and morphology was studied using NG108-15 neuronal cells. Cell

viability was measured by quantifying live versus dead cells. There was no statistical difference between cells grown on the neat versus blend fiber samples, suggesting that all gyrospun PHA fibers supported the attachment and proliferation of the cells (**Figure S13**).

Confocal micrographs of NG108-15 neuronal cells cultured on all the gyrospun PHA fibers stained positively for β-III tubulin, confirming neurite extensions, which grew in an aligned manner, following the fibers (**Figure 8**).

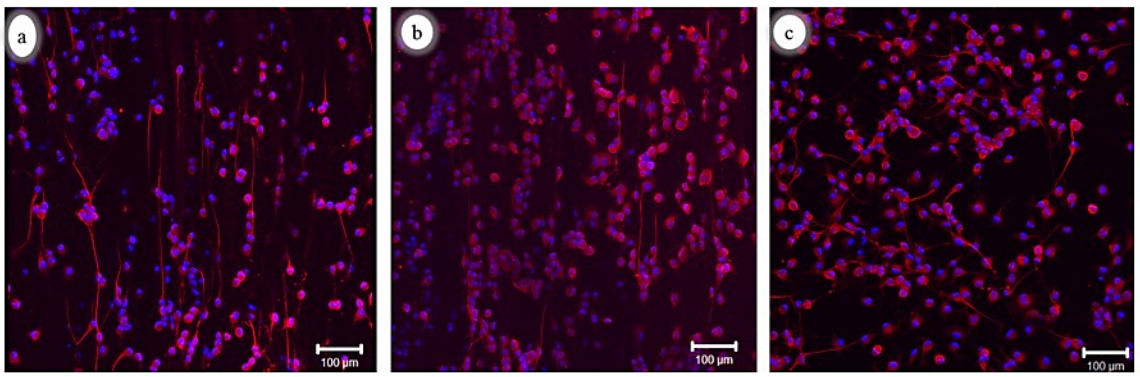

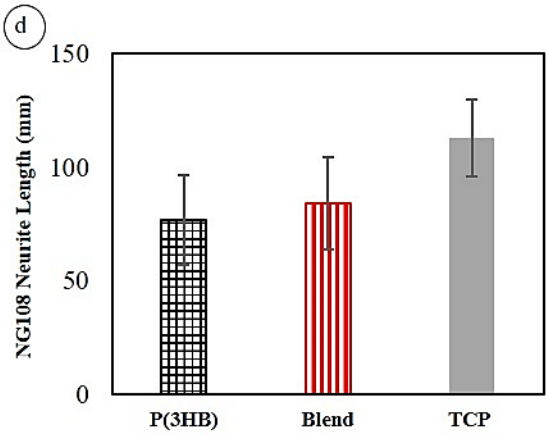

Figure 8: Neuronal cell differentiation on gyrospun PHA fibers. Confocal micrographs of NG108-15 neuronal cells cultured on (a) P(3HB) fibers, (b) P(3HB)/P(3HO-*co*-3HD) fibers and (c) TCP. Neuronal cell nuclei were labelled with DAPI (blue) and neurites were stained with β III tubulin, to show neurite extensions, lengths and direction of growth identified (red). NG108-15 neuronal cells cultured on the fibers expressed neurites. Scale bar =100µm. (d) average neurite length of NG108-15 neuronal cells cultured on P(3HB), P(3HB)/ P(3HO-*co*-3HD) blend fibers and TCP.

The longest average neurite lengths were detected when cells were cultured on the P(3HB)/P(3HO-*co*-3HD) blend fibers (83.9 ± 20.4μm), followed by those cultured on the P(3HB) fibers (76.9 ± 19.8μm) respectively. There was no statistical difference between the average neurite lengths expressed by neuronal cells on the fiber samples. This indicated that all the gyrospun PHA fibers were able to support NG108-15 neuronal cell differentiation. Furthermore, the morphology of rat primary Schwann cells cultured on the gyrospun PHA fibers was also assessed (**Figure 9, Figure**

S14). Schwann cells adhered to the fibers and elongated on both the fiber samples in an aligned manner. No statistical differences were detected between cells grown on the P(3HB) and P(3HB)/P(3HO-*co*-3HD) blend fibers, and both conditions supported higher than 95% cell viability.

Previous experimental studies suggest that primary Schwann cells attach and migrate faster on aligned fibers in comparison to the randomly oriented fibers or flat films.[58, 59] Schwann cell length is a known marker to determine whether Schwann cells retain their phenotype when cultured on the fibers.[58, 59]

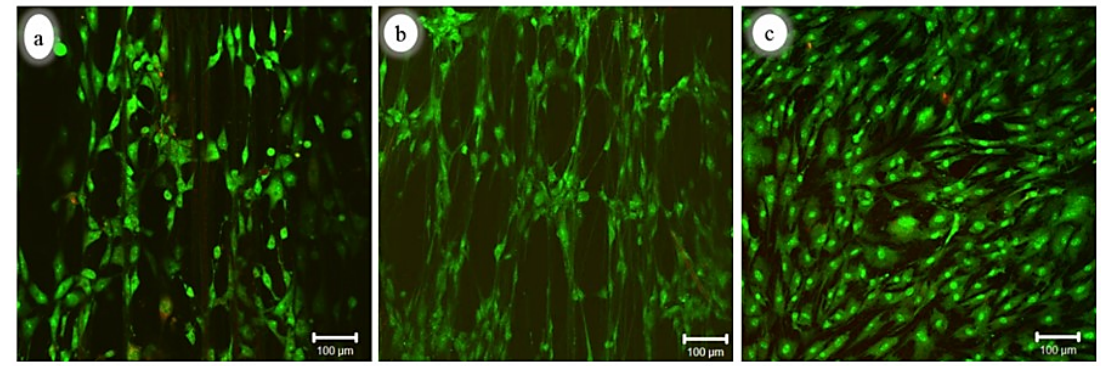

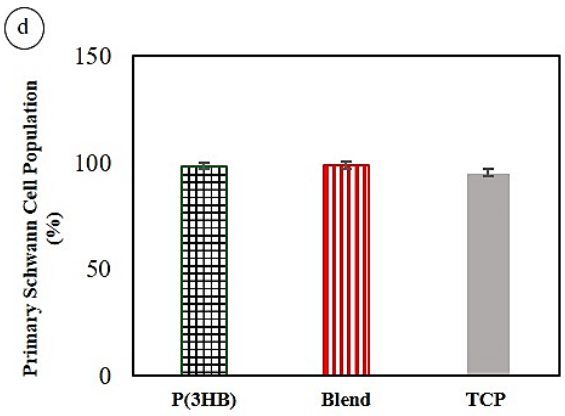

Figure 9: Analysis of rat primary Schwann cells cultured on the gyrospun PHA fibers. Confocal micrographs of rat primary Schwann cells cultured on (a) P(3HB), (b) P(3HB)/P(3HO-co-3HD) blend fibers and (c) TCP (Scale bar =100µm). (d) Images were quantified to determine the live cell and dead cell numbers, per field of view (841µm x 841µm), for each condition, and expressed as a percentage. (mean ± SD, n=3 independent experiments).

In this study, the Schwann cell length on the P(3HB)/P(3HO-*co*-3HD) 80:20 blend fibers were 76.1± 14.9 μm and 74.4 ± 15.7μm on the P(3HB) fibers. There was no statistical difference, indicating that the Schwann cells cultured on both gyrospun PHA fibers maintained their morphology (**Figures 9 & S14**). Both P(3HB) and P(3HB)/P(3HO-*co*-3HD) blend fibers were thus found to be biocompatible and confirmed as a suitable biomaterial for nerve regeneration without the aid of any nerve growth factors.

3.4.1. Evaluation of Gyrospun PHA Fibers Using a Pre-Clinical 3D Dorsal Root Ganglion (DRG) Ex Vivo Model: A 3D *ex vivo* model uses the dorsal root ganglion to mirror the proximal nerve

stump after nerve injury, as described in Behbehani *et al*., 2018.[19,39] It is an efficient tool to assess the internal fiber scaffolds for their ability to promote axon regeneration. Gyrospun aligned PHA fibers were placed within polyethylene glycol nerve conduits fabricated by microstereolithography, as described in Behbehani *et al*., 2018.[19, 39] After 7 days of culture, axons and Schwann cells grew from the proximal DRG body along the gyrospun PHA fibers placed inside 5 mm long conduits. Both P(3HB) and P(3HB)/P(3HO-*co*-3HD) 80:20 blend fibers supported the outgrowth of the two cell types as shown in **Figure 10**.

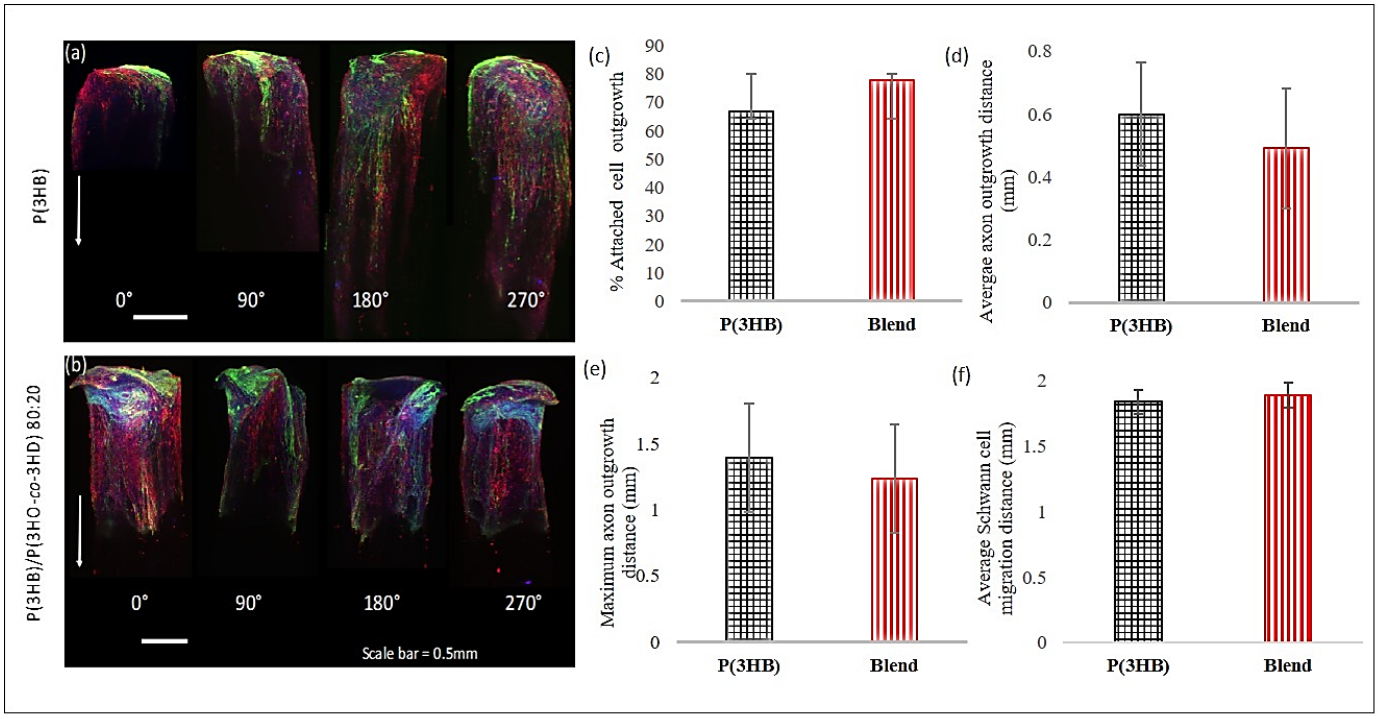

Figure 10: Light-sheet microscopy images showing the outgrowth of axons (ß-III tubulin, green) and Schwann cells (S100ß, red) along aligned (a) P(3HB) fibers and (b) P(3HB)/P(3HO-*co*-3HD) 80:20 blend gyrospun fibers inside a 5 mm long polyethylene glycol conduit. Nuclei were labelled with DAPI (blue). Images are shown as maximum projections with multiple views stitched together. Outgrowth was captured in four angles using a 90° rotation (0°, 90°, 180°, 270° from left to right). Arrows indicate outgrowth direction. Representative images shown of three independently repeated experiments. Scale bar = 0.5 mm. (c) % attached cell outgrowth on the P(3HB) and P(3HB)/P(3HO-co-3HD) 80:20 blend gyrospun fibers. (d) Average axon outgrowth distance (mm) P(3HB) and P(3HB)/P(3HO-co-3HD) 80:20 blend gyrospun fibers. (e) Maximum axon outgrowth distance (mm) on the P(3HB) and P(3HB)/P(3HO-co-3HD) 80:20 blend gyrospun fibers. (f) Average Schwann cell migration distance (mm) on the P(3HB) and P(3HB)/P(3HO-co-3HD) 80:20 blend gyrospun fibers.

It was noted that axons and Schwann cells on P(3HB) fibers grew preferably on one side of the scaffold (**Figure 10a**) in comparison to the cells on the P(3HB)/P(3HO-*co*-3HD) blend fibers, which showed an even outgrowth along all four sides of the scaffold (**Figure 10b**). In addition to these differences, a longer outgrowth distance was noticed on P(3HB) fibers than on P(3HB)/P(3HO-*co*-3HD) blend fibers. Axons were always co-localized with Schwann cells, whereas Schwann cells were also detected without the presence of axons. Further quantification confirmed that both fiber samples performed equally well in supporting axon outgrowth. In over 60 % of all attached DRGs, an outgrowth of axons and Schwann cells was detected, from which 66.6 ± 0% and 77.8 ± 19.3 % grew out on P(3HB) and P(3HB)/P(3HO-*co*-3HD) blend fibers respectively (**Figure 10c**), but with no significant differences. The average axon outgrowth per fiber samples measured 0.6 ± 0.2 mm and 0.5 ± 0.2 mm on P(3HB) and P(3HB)/P(3HO-*co*-3HD) 80:20 blend fibers respectively (**Figure 10d**). The longest axons were detected on P(3HB) fibers with a maximum outgrowth of 1.4 ± 0.4 mm. In comparison, the average maximum axon outgrowth measured 1.2 ± 0.4 mm on the P(3HB)/P(3HO-*co*-3HD) 80:20 blend fibers (**Figure 10e**). However, no statistical differences could be identified. The average Schwann cell migration per fiber sample measured 1.84 ± 0.18 and 1.89 ± 0.19 on P(3HB) and P(3HB)/P(3HO-*co*-3HD) 80:20 blend fibers respectively with no significant differences (**Figure 10f**). The DRG data substantiated the potential of the aligned gyrospun PHA fibers as promising intraluminal fiber scaffolds for efficient nerve regeneration. Gyrospinning has allowed the efficient use of the otherwise stiff and relatively more processable PHA, P(3HB), for nerve tissue engineering, a soft tissue replacement, an unusual and unexpected result.

3.5. Cardiovascular tissue engineering: Unlike bone and peripheral nerves, the heart has a limited capacity for repair. The ideal clinical intervention would be creation of a viable myocardial tissue to replace scar tissue post myocardial infarction and restore cardiac function.[60,61] Considerable effort is being made to design and fabricate 3D scaffolds to act as substrates for cardiac tissue regenerative patches.[62, 63] In this study, we have investigated the properties of gyrospun P(3HB) and P(3HB)/P(3HO-*co*-3HD) blend fibers as potential scaffolds for cardiovascular tissue regeneration.

3.5.1. In Vitro Response of the Gyrospun PHA Fibers when Seeded with Human Induced Pluripotent Stem Cell Derived Cardiomyocytes (hiPSC-CMs): hiPSC-CMs are a clinically relevant *in vitro* model system in cardiovascular research and are also a convincing cell source for contractile cardiac muscle. hiPSC-CMs retain the ultrastructural and functional properties of native (albeit immature) cardiomyocytes in long-term

culture and can be formed into sheets of tissue with synchronized contractions.[64-66] In this study, cell-scaffold interaction was studied by culturing hiPSC-CMs on the gyrospun P(3HB) and P(3HB)/P(3HO-*co*-3HD) 80:20 blend fibers (random and aligned) for 24 hours. Cell viability was measured by quantifying the average number of live and dead cells on the fibers (**Figure S15**). Confocal micrographs of the cell seeded scaffolds demonstrated cell attachment and confluent coverage of the scaffolds. Live cell percentage was higher than 90% on all the gyrospun PHA fibers. There was no statistical difference between neat and blend fiber scaffolds. Furthermore, nuclei alignment of the hiPSC-CM cells cultured on both random and aligned P(3HB) and P(3HB)/P(3HO-3HD) blend fiber constructs was quantified using α-actinin + DAPI staining (**Figure S15**). From the representative images, it was evident that the hiPSC-CMs seeded on the aligned fibers exhibited directionality compared to those cultured on the random fibers. Underlying aligned gyrospun PHA fibers provided guidance cues to the hiPSC-CMs to obtain anisotropic orientation. There was a statistical difference between the alignment of the cells on the aligned versus random fibers (**Figure S15**). Previous studies have proposed that cell alignment promotes cardiomyocyte maturation, which is essential in regenerating anisotropic heart tissue.[67-70] In an adult myocardium, cardiomyocytes are arranged in aligned parallel bundles that expedite mechanical contraction and electrical propagation necessary for cardiac function.[71] As revealed by the α-actinin at the z line, hiPSC-CMs seeded on the aligned gyrospun P(3HB) and P(3HB)/P(3HO-*co*-3HD) blend fibers exhibited well defined sarcomere alignment, which is one of the key characteristics of adult cardiomyocytes as shown in **Figure 11**.[72] hiPSC-CMs demonstrated a modulus angle of **45°** from the mean axis on P(3HB) fibers, whilst a modulus angle of **50°** from the mean axis was observed on the P(3HB)/P(3HO-*co*-3HD) blend fibers (**Figure S15**).

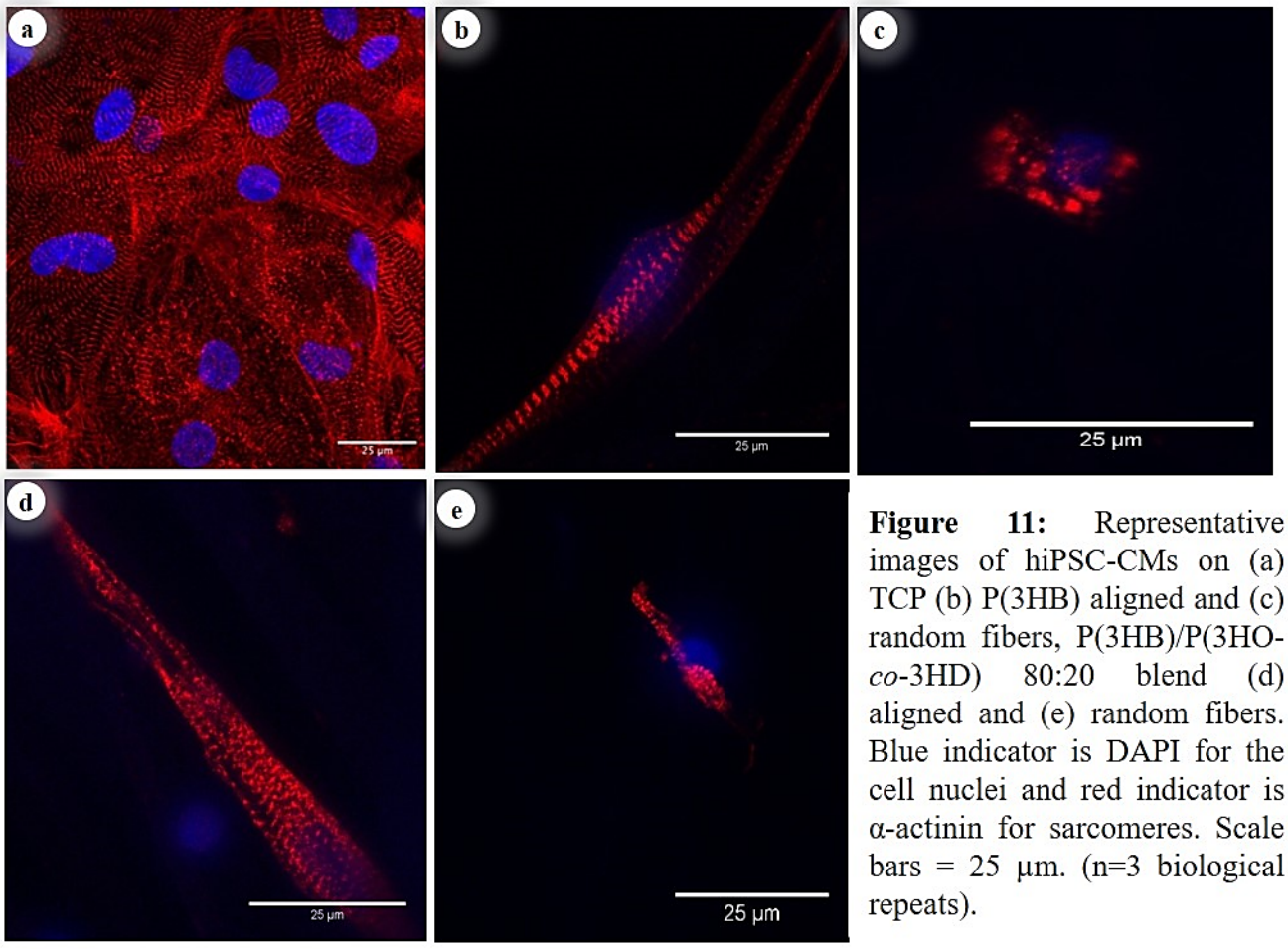

Figure 11: Representative images of hiPSC-CMs on (a) TCP (b) P(3HB) aligned and (c) random fibers, P(3HB)/P(3HO-*co*-3HD) 80:20 blend (d) aligned and (e) random fibers. Blue indicator is DAPI for the cell nuclei and red indicator is α-actinin for sarcomeres. Scale bars = 25 µm. (n=3 biological repeats).

2.5.2. Effect of hiPSC-CM Calcium Handling on Gyrospun PHA Fibers: Previous studies have revealed that an adult cardiomyocyte exhibits a well-defined cascade of events with regards to calcium handling.[72] The effect of the fiber alignment on the cardiomyocyte function such as calcium handling was studied as shown in **Figure 12**. The hiPSC-CMs cultured on the gyrospun PHA fibers displayed functional calcium uptake with the release mechanism detected by addition of the calcium sensitive fluo-4 AM dye to the cells prior to the test (**Figure 12**). No statistical difference was observed in the peak amplitude, and time to 50% decay in the hiPSC-CMs cultured on the gyrospun P(3HB) and P(3HB)/P(3HO-*co*-3HD) blend fibers (random and aligned). However, there was a significant reduction in the time to peak and in the time to 90% decay in the hiPSC-CMs cultured on the aligned fibers in comparison to those on the random fibers. Shorter calcium transient duration indicated that the calcium handling was enhanced in the hiPSC-CMs cultured on the aligned fibers, which was representative of an adult/mature phenotype.[71, 73, 74]

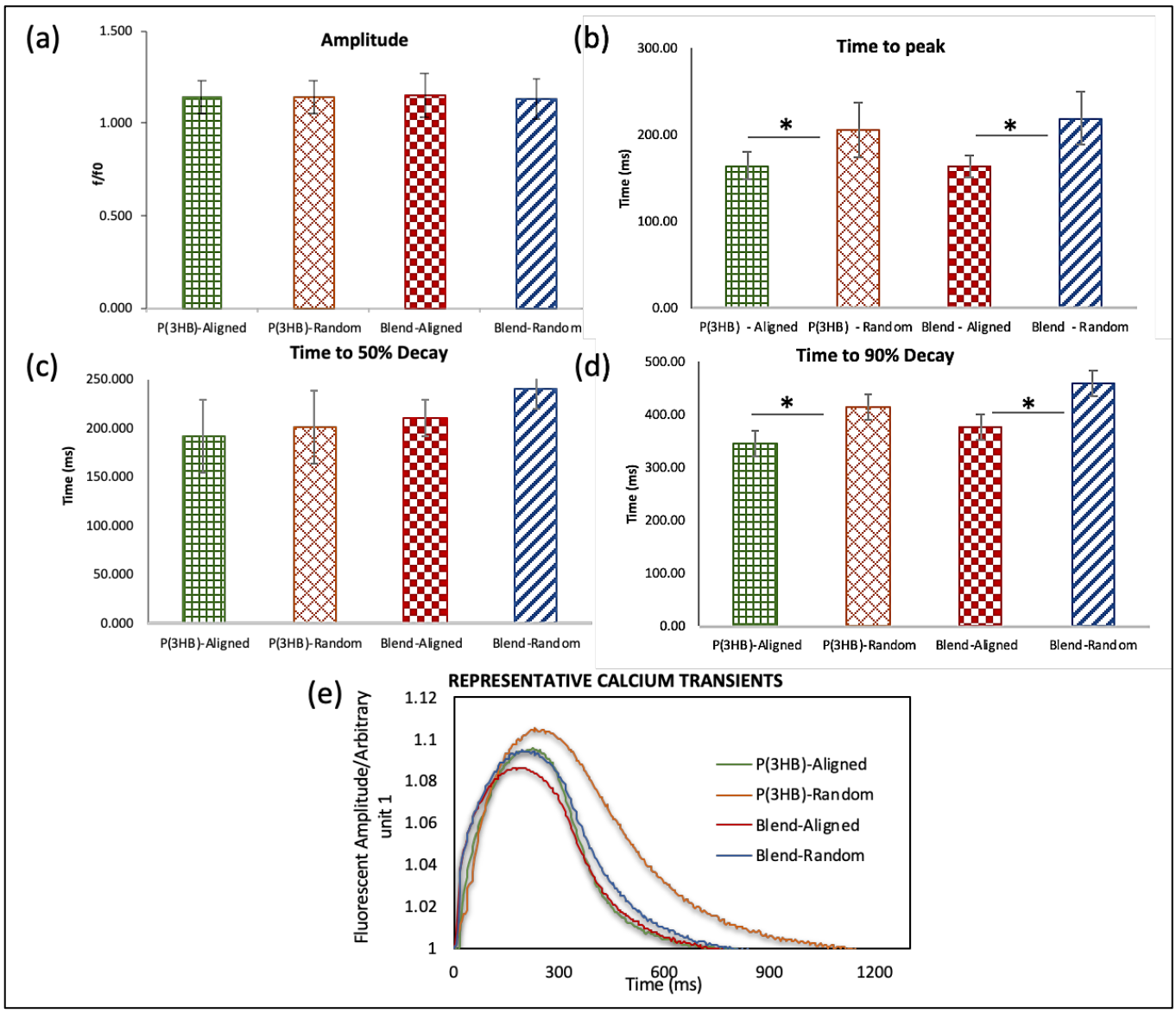

Figure 12: Effect of the gyrospun PHA fibers on iPSC-CM calcium handling (a) amplitude, (b) T_p, (c) T_{50} and (d) T_{90} of the calcium transients in cells field stimulated at 1Hz. (e) representative calcium transient traces at 1 Hz stimulation. (n= 3 biological repeat).

The results of this study demonstrated that the aligned gyrospun PHA fibers promoted hiPSC-CM maturation. Furthermore, the novel application and potential of gyrospinning of P(3HB), the relatively stiff PHA, for cardiac TE, a soft tissue replacement, has been successfully demonstrated.

4. Conclusion: This study has, for the first time, established beyond doubt the significant potential of gyrospun PHA fiber scaffolds for both hard (bone) and soft (nerve and cardiovascular) tissue engineering, without the requirement for additional growth factors. A highly effective and

scalable toolbox has been created which can be used for the regeneration of a wide range of tissue types with significant translational and clinical potential, an excellent and promising outcome for an increasingly ageing demographic.

Supporting Information:

- Temporal profiles for the production of PHAs; characterisation data of the PHAs produced (GC-MS, NMR, DSC, GPC).
- Bone: Alkaline Phosphatase and Pico Green dsDNA quantitation data, EDX spectra of the gyrospun fibres incubated in SBF, Histological data for *in vivo* bone regeneration and control CAM data without scaffold.
- Nerve: Cell viability data and confocal micrographs of NG108-15 neuronal and primary Schwann cell phenotype on gyrospun fibres.
- Cardiac: Confocal micrographs of hiPSC-CMs on gyrospun fibres.

AUTHOR INFORMATION

Corresponding Author
*Email: I.Roy@sheffield.ac.uk
Phone: +44(0)1142225962

Author Contributions

The contributions of the authors of this article are (a) participation in the research: P.B., R.K.M., U.I., J.D., J.M.K., C.S.T., M.B., E.H., Q.M., B.L., R.N., R.O.C.O., J.W.H., C.T., S.E.H., M.E. and I.R. (b) article preparation: P.B, R.K.M and I.R. (c) Design of experiments: I.R. and P.B. (d) Data Collection: P.B., R.K.M., U.I., J.D., J.M.K., C.S.T., M.B., E.H., Q.M., B.L., R.N., R.O.C.O., J.W.H., C.T., S.E.H., M.E. and I.R. (e) Data analysis and interpretation: P.B., R.K.M., U.I., J.D., J.M.K., C.S.T., M.B., E.H., Q.M., B.L., R.N., R.O.C.O., J.W.H., C.T., S.E.H., M.E. and I.R.(f) Compilation of the article: P.B, R.K.M. and I.R. (g) Approval of the final version of the article: All the authors edited the final submission. P.B. and R.K.M contributed equally and are the first authors.

Funding

The work was supported by the ReBioStent project European 807 Union's Seventh Programme for research, technological development and demonstration under grant agreement no. 604251 (P.B., B.L., I.R.), the Neurimp project under grant agreement no. 604450 (P.B., R.N, I.R.), H2020 project POLYBIOSKIN under grant agreement no. 745839 (P.B., I.R.) and British Heart Foundation Centre of Regenerative Medicine, Imperial College London [BHF RM/17/1/33377] (I.R.). R.O.C.O, J.I.D and J.M.K. gratefully acknowledges financial support from the Biotechnology and Biological Sciences Research Council (BB/P017711/1) and the UK Regenerative Medicine Platform "Acellular / Smart Materials – 3D Architecture" (MR/R015651/1). S.E.H., Q.M., E.H. and C.T. acknowledge funding provided by the British Heart Foundation Centre of Regenerative Medicine, Imperial College London [BHF

RM/17/1/33377]. J.W.H. and C.S.T. acknowledge funding provided by the FP7 NEURIMP grant [grant agreement ID: 604450]. M.E., R.K.M. and U.I. acknowledge funding from the Engineering & Physical Sciences Research Council, UK [grants EP/S016872/1, EP/N034228/1, EP/L023059/1].

Notes

All authors have approved the final article. The authors declare no competing financial interest.

Acknowledgements

We are thankful to the staff at the University of Westminster for their help with the fermentation process. We thank J Wells, Bone and Joint Research Group, University of Southampton for technical support.

REFERENCES

1. Rose, J. C.; De Laporte, L. Hierarchical Design of Tissue Regenerative Constructs. Advanced Healthcare Material 2018, 7, 1701067.

2. Nikolova, M. P.; Murthy S. C. Recent Advances in Biomaterials for 3D scaffolds: A Review. Bioactive Materials 2019, 4, 271-292.

3. Patil, V. A.; Kristyn S. M. Engineered Collagen Matrices. Bioengineering 2020, 7(4), 163.

4. Ghasemi-Mobarakeh, L.; Prabhakaran, M. P.; Tian, L.; Shamirzaei-Jeshvaghani, E.; Dehghani, L.; Ramakrishna, S. Structural Properties of Scaffolds: Crucial Parameters Towards Stem Cells Differentiation. World Journal of Stem Cells 2015, 7, 728-744.

5. Lakshmanan, R.; Krishnan, U. M.; Sethuraman, S. Polymeric Scaffold Aided Stem Cell Therapeutics for Cardiac Muscle Repair and Regeneration. Macromolecular Bioscience 2013, 13, 1119-1134.

6. Koller, M. Biodegradable and Biocompatible Polyhydroxyalkanoates (PHA): Auspicious Microbial Macromolecules for Pharmaceutical and Therapeutic Applications. Molecules 2018, 23, 362.

7. Nigmatullin, R.; Thomas, P.; Lukasiewicz, B.; Puthussery, H.; Roy, I. Polyhydroxyalkanoates, a Family of Natural Polymers, and their Applications in Drug Delivery. Journal of Chemical Technology and Biotechnology 2015, 90, 1209-122.

8. Basnett, P.; Lukasiewicz, B.; Marcello, E.; Gura, H. K.; Knowles, J. C.; Roy, I. Production of a Novel Medium Chain Length Poly(3-hydroxyalkanoate) using Unprocessed Biodiesel Waste and its Evaluation as a Tissue Engineering Scaffold. Microbial Biotechnology 2017, 10, 1384-1399.

9. Kalia, V. C. Biotechnological Applications of Polyhydroxyalkanoates; Springer Singapore Pte. Limited: Singapore, 2019.

10. Lukasiewicz, B.; Basnett, P.; Nigmatullin, R.; Matharu, R.; Knowles, J. C.; Roy, I. Binary Polyhydroxyalkanoate Systems for Soft Tissue Engineering. Acta Biomaterialia 2018, 71, 225-234.

11. Eltom, A.; Zhong, G.; Muhammad, A. Scaffold Techniques and Designs in Tissue Engineering Functions and Purposes: A Review. Advances in Materials Science and Engineering 2019, 2019, 1-13.

12. Hutmacher, D. W. Scaffold Design and Fabrication Technologies for Engineering Tissues-State of the Art and Future Perspectives. Journal of Biomaterials Science, Polymer Edition 2001, 12, 107-124.

13. Mahalingam, S.; Edirisinghe, M. Forming of Polymer Nanofibers by a Pressurised Gyration Process. Macromolecular Rapid Communications 2013, 34, 1134-1139.

14. Timin, A. S.; Muslimov, A. R.; Zyuzin, M. V.; Peltek, O. O.; Karpov, T. E.; Sergeev, I. S.; Dotsenko, A. I.; Goncharenko, A. A.; Yolshin, N. D.; Sinelnik, A.; Krause, B.; Baumbach, T.; Surmeneva, M. A.; Chernozem, R. V.; Sukhorukov, G. B.; Surmenev, R. A. Multifunctional Scaffolds with Improved Antimicrobial Properties and Osteogenicity Based on Piezoelectric Electrospun Fibers Decorated with Bioactive Composite Microcapsules. ACS Applied Materials & Interfaces 2018, 10, 34849-34868.

15. Karpov, T. E.; Peltek, O. O.; Muslimov, A. R.; Tarakanchikova, Y. V.; Grunina, T. M.; Poponova, M. S.; Karyagina, A. S.; Chernozem, R. V.; Pariy, I. O.; Mukhortova, Y. R.; Zhukov, M. V.; Surmeneva, M. A.; Zyuzin, M. V.; Timin, A. S.; Surmenev, R. A. Development of Optimized Strategies for Growth Factor Incorporation onto Electrospun Fibrous Scaffolds To Promote Prolonged Release. ACS Applied Materials & Interfaces 2020, 12, 5578-5592.

16. Ahmed, J.; Matharu, R. K.; Shams, T.; Illangakoon, U. E.; Edirisinghe, M. A Comparison of Electric-Field-Driven and Pressure-Driven Fiber Generation Methods for Drug Delivery. Macromolecular Materials and Engineering 2018, 303, 1700577.

17. Basnett, P.; Marcello, E.; Lukasiewicz, B.; Nigmatullin, R.; Paxinou, A.; Ahmad, M. H.; Gurumayum, B.; Roy, I. Antimicrobial Materials with Lime Oil and a Poly(3-hydroxyalkanoate) Produced via Valorisation of Sugar Cane Molasses. Journal of Functional Biomaterials 2020, 11, 24.

18. Moreno-Jiménez, I.; Hulsart-Billstrom, G.; Lanham, S. A.; Janeczek, A. A.; Kontouli, N.; Kanczler, J. M.; Evans, N. D.; Oreffo, R. O. The Chorioallantoic Membrane (CAM) Assay for the Study of Human Bone Regeneration: a Refinement Animal Model for Tissue Engineering. Scientific Reports 2016, 6, 32168.

19. Behbehani, M.; Glen, A.; Taylor, C. S.; Schuhmacher, A.; Claeyssens, F.; Haycock, J. W. Pre-clinical Evaluation of Advanced Nerve Guide Conduits using a Novel 3D In Vitro Testing Model. International Journal of Bioprinting 2018, 4, 123.

20. Sandoval-Castellanos, A. M.; Claeyssens, F.; Haycock, J. W. Biomimetic Surface Delivery of NGF and BDNF to Enhance Neurite Outgrowth. Biotechnology and Bioengineering 2020, 117, 3124-3135.

21. Maldonado, R. F.; Sá-Correia, I.; Valvano, M. A. Lipopolysaccharide Modification in Gram-Negative Bacteria during Chronic Infection. FEMS Microbiology Reviews 2016, 40, 480-493.

22. Valappil, S. P.; Peiris, D.; Langley, G. J.; Herniman, J. M.; Boccaccini, A. R.; Bucke, C.; Roy, I. Polyhydroxyalkanoate (PHA) Biosynthesis from Structurally Unrelated Carbon Sources by a Newly Characterized Bacillus spp. Journal of Biotechnology 2007, 127, 475-487.

23. Basnett, P.; Marcello, E.; Lukasiewicz, B.; Panchal, B.; Nigmatullin, R.; Knowles, J. C.; Roy, I. Biosynthesis and Characterization of a Novel, Biocompatible Medium Chain Length Polyhydroxyalkanoate by *Pseudomonas mendocina* CH50 using Coconut Oil as the Carbon Source. J. Mater. Sci: Mat. Med 2018, 29, 1-11.

24. Constantinides, C.; Basnett, P.; Lukasiewicz, B.; Carnicer, R.; Swider, E.; Majid, Q. A.; Srinivas, M.; Carr, C. A.; Roy, I. In Vivo Tracking and 1H/19F Magnetic Resonance Imaging of Biodegradable Polyhydroxyalkanoate/Polycaprolactone Blend Scaffolds Seeded with Labeled Cardiac Stem Cells. ACS Applied Materials & Interfaces 2018, 10, 25056-25068.

25. Fonck, E.; Feigl, G. G.; Fasel, J.; Sage, D.; Unser, M.; Rüfenacht, D. A.; Stergiopulos, N.

Effect of Aging on Elastin Functionality in Human Cerebral Arteries. Stroke 2009, 40, 2552-2556.

26. Illangakoon, U. E.; Mahalingam, S.; Matharu, R. K.; Edirisinghe, M. Evolution of Surface Nanopores in Pressurised Gyrospun Polymeric Microfibers. Polymers 2017, 9, 508.

27. Srinivasarao, M. Three-Dimensionally Ordered Array of Air Bubbles in a Polymer Film. Science 2001, 292, 79-83.

28. Cai, Y.; Zhang Newby, B. Porous Polymer Films Templated by Marangoni Flow-Induced Water Droplet Arrays. Langmuir 2009, 25, 7638-7645.

29. Maruyama, N.; Koito, T.; Nishida, J.; Sawadaishi, T.; Cieren, X.; Ijiro, K.; Karthaus, O.; Shimomura, M. Mesoscopic Patterns of Molecular Aggregates on Solid Substrates. Thin Solid Films 1998, 327-329, 854-856.

30. Wan, L.; Zhu, L.; Ou, Y.; Xu, Z. Multiple Interfaces in Self-assembled Breath Figures. Chemical Communications 2014, 50, 4024-4039.

31. Zhang, A.; Bai, H.; Li, L. Breath Figure: A Nature-Inspired Preparation Method for Ordered Porous Films. Chemical Reviews 2015, 115, 9801-9868.

32. Munj, H.; Tomasko, D. Polycaprolactone-Polymethyl Methacrylate Electrospun Blends for Biomedical Applications. Polym. Sci. Ser. A 2017*, 59*, 695-707.

33. Boger, A.; Bisig, A.; Bohner, M.; Heini, P.; Schneider, E. Variation of the Mechanical Properties of PMMA to Suit Osteoporotic Cancellous Bone. Journal of Biomaterials Science, Polymer Edition 2012, 19, 1125-1142.

34. Eshraghi, S.; Das, S. Mechanical and Microstructural Properties of Polycaprolactone Scaffolds with One-Dimensional, Two-Dimensional, and Three-Dimensional Orthogonally Oriented Porous Architectures Produced by Selective Laser Sintering. Acta Biomater 2010, 6(7), 2467-76.

35. Feltz, K. P.; Kalaf, E. A. G.; Chen, C.; Martin, R. S.; Sell, S. A. A Review of Electrospinning Manipulation Techniques to Direct Fiber Deposition and Maximize Pore Size. Electrospinning 2017, 1, 46-61.

36. Wang, X.; Lou, T.; Zhao, W.; Song, G.; Li, C.; Cui, G. The Effect of Fiber Size and Pore Size on Cell Proliferation and Infiltration in PLLA Scaffolds on Bone Tissue Engineering. Journal of Biomaterials Applications 2016, 30, 1545-1551.

37. Guo, Z.; Ma, M.; Huang, X.; Li, H.; Zhou, C. Effect of Fiber Diameter on Proliferation and Differentiation of MC3T3-E1 Pre-Osteoblasts. Journal of Biomaterials and Tissue Engineering 2017, 7, 162-169.

38. MacNeil, S. Progress and Opportunities for Tissue-Engineered Skin. Nature 2007, 445, 874-880.

39. Daud, M. F. B.; Pawar, K. C.; Claeyssens, F.; Ryan, A. J.; Haycock, J. W. An Aligned 3D Neuronal-Glial Co-Culture Model for Peripheral Nerve Studies. Biomaterials 2012, 33, 5901-5913.

40. Pateman, C. J.; Harding, A. J.; Glen, A.; Taylor, C. S.; Christmas, C. R.; Robinson, P. P.; Rimmer, S.; Boissonade, F. M.; Claeyssens, F.; Haycock, J. W. Nerve Guides Manufactured from Photocurable Polymers to Aid Peripheral Nerve Repair. Biomaterials 2015, 49, 77-89.

41. Qazi, T. H.; Mooney, D. J.; Pumberger, M.; Geißler, S.; Duda, G. N. Biomaterials Based Strategies for Skeletal Muscle Tissue Engineering: Existing Technologies and Future Trends. Biomaterials 2015, 53, 502-521.

42. Parrag, I. C.; Zandstra, P. W.; Woodhouse, K. A. Fiber Alignment and Coculture With Fibroblasts improves the Differentiated Phenotype of

Murine Embryonic Stem Cell-Derived Cardiomyocytes for Cardiac Tissue Engineering. Biotechnology and Bioengineering 2012, 109, 813-822.

43. Delaine-Smith, R. M.; Green, N. H.; Matcher, S. J.; MacNeil, S.; Reilly, G. C. Monitoring Fibrous Scaffold Guidance of Three-Dimensional Collagen Organisation Using Minimally-Invasive Second Harmonic Generation. PloS One 2014, 9, e89761.

44. Gray, B.; Lieu, D.; Collins, S.; Smith, R.; Barakat, A. Microchannel Platform for the Study of Endothelial Cell Shape and Function. Biomedical Microdevices 2002, 4, 9-16.

45. Ho-Shui-Ling, A.; Bolander, J.; Rustom, L. E.; Johnson, A. W.; Luyten, F. P.; Picart, C. Bone Regeneration Strategies: Engineered Scaffolds, Bioactive Molecules and Stem Cells Current Stage and Future Perspectives. Biomaterials 2018, 180, 143-162.

46. Calabrese, G.; Giuffrida, R.; Fabbi, C.; Figallo, E.; Lo Furno, D.; Gulino, R.; Colarossi, C.; Fullone, F.; Giuffrida, R.; Parenti, R.; Memeo, L.; Forte, S. Collagen-Hydroxyapatite Scaffolds Induce Human Adipose Derived Stem Cells Osteogenic Differentiation In Vitro. PloS One 2016, 11, e0151181.

47. Dalby, M. J.; Di Silvio, L.; Harper, E. J.; Bonfield, W. Initial Interaction of Osteoblasts with the surface of a Hydroxyapatite-Poly(Methylmethacrylate) Cement. Biomaterials 2001, 22, 1739-1747.

48. Chen, W.; Sun, Y.; Fu, J. Nanotopological Surfaces: Microfabricated Nanotopological Surfaces for Study of Adhesion-Dependent Cell Mechanosensitivity (Small 1/2013). Small (Weinheim an der Bergstrasse, Germany) 2013, 9, 1.

49. Dalby, M. J.; Yarwood, S. J.; Riehle, M. O.; Johnstone, H. J. H.; Affrossman, S.; Curtis, A. S. G. Increasing Fibroblast Response to Materials using Nanotopography: Morphological and Genetic Measurements of Cell Response to 13-nm-High Polymer Demixed Islands. Experimental Cell Research 2002, 276, 1-9.

50. Kyllönen, L.; Haimi, S.; Mannerström, B.; Huhtala, H.; Rajala, K. M.; Skottman, H.; Sándor, G. K.; Miettinen, S. Effects of Different Serum Conditions on Osteogenic Differentiation of Human Adipose Stem Cells In Vitro. Stem Cell Research & Therapy 2013, 4, 17.

51. Florea, D. A.; Chircov, C.; Grumezescu, A. M. Hydroxyapatite Particles Directing the Cellular Activity in Bone Regeneration Processes: An Up-To-Date Review. Applied Sciences 2020, 10, 3483.

52. Kokubo, T.; Takadama, H. How Useful is SBF in Predicting In Vivo Bone Bioactivity? Biomaterials 2006, 27, 2907-2915.

53. Gothard, D.; Smith, E. L.; Kanczler, J. M.; Black, C. R.; Wells, J. A.; Roberts, C. A.; White, L. J.; Qutachi, O.; Peto, H.; Rashidi, H.; Rojo, L.; Stevens, M. M.; El Haj, A. J.; Rose, Felicity R. A. J; Shakesheff, K. M.; Oreffo, R. O. C. In Vivo Assessment of Bone Regeneration in Alginate/Bone ECM Hydrogels with Incorporated Skeletal Stem Cells and Single Growth Factors. PloS One 2015, 10, e0145080.

54. Kanczler, J. M.; Oreffo, R. O. C. Osteogenesis and Angiogenesis: The Potential for Engineering Bone. European Cells & Materials 2008, 15, 100-114.

55. Boomsma, R. A.; Geenen, D. L. Mesenchymal Stem Cells Secrete Multiple Cytokines that Promote Angiogenesis and have Contrasting Effects on Chemotaxis and Apoptosis. PloS One 2012, 7, e35685.

56. Croes, M.; Kruyt, M. C.; Groen, W. M.; Van Dorenmalen, K. M. A; Dhert, W. J. A.; Öner, F. C.; Alblas, J. Interleukin 17 Enhances Bone Morphogenetic Protein-2-Induced Ectopic Bone Formation. Scientific Reports 2018, 8, 7269-13.

57. Bell, J. H. A.; Haycock, J. W. Next Generation Nerve Guides: Materials, Fabrication, Growth Factors, and Cell Delivery. Tissue Engineering. Part B, Reviews 2012, 18, 116-128.

58. Radhakrishnan, J.; Kuppuswamy, A. A.; Sethuraman, S.; Subramanian, A. Topographic Cue from Electrospun Scaffolds Regulate Myelin-Related Gene Expressions in Schwann Cells. Journal of Biomedical Nanotechnology 2015, 11, 512-521.

59. Chew, S. Y.; Mi, R.; Hoke, A.; Leong, K. W. The Effect of the Alignment of Electrospun Fibrous Scaffolds on Schwann Cell Maturation. Biomaterials 2008, 29, 653-661.

60. Curtis, M.W.; Russell, B. Cardiac Tissue Engineering. J. Cardiovasc. Nurs. 2009, 24(2), 87-92.

61. Nguyen, A. H.; Marsh, P.; Schmiess-Heine, L.; Burke, P. J.; Lee, A.; Lee, J.; Cao, H. Cardiac Tissue Engineering: State-Of-The-Art Methods and Outlook. Journal of Biological Engineering 2019, 13, 57.

62. Heydarkhan-Hagvall, S.; Schenke-Layland, K.; Dhanasopon, A. P.; Rofail, F.; Smith, H.; Wu, B. M.; Shemin, R.; Beygui, R. E.; MacLellan, W. R. Three-Dimensional Electrospun ECM-Based Hybrid Scaffolds for Cardiovascular Tissue Engineering. Biomaterials 2008, 29, 2907-2914.

63. Kitsara, M.; Agbulut, O.; Kontziampasis, D.; Chen, Y.; Menasché, P. Fibers for Hearts: A Critical Review on Electrospinning for Cardiac Tissue Engineering. Acta Biomaterialia 2017, 48, 20-40.

64. Zwi, L.; Caspi, O.; Arbel, G.; Huber, I.; Gepstein, A.; Park, I.; Gepstein, L. Cardiomyocyte Differentiation of Human Induced Pluripotent Stem Cells. Circulation 2009, 120, 1513-1523.

65. Balafkan Novin; Mostafavi Sepideh; Schubert Manja; Siller Richard; Liang Kristina Xiao; Sullivan Gareth; Bindoff Laurence, A. A Method for Differentiating Human Induced Pluripotent Stem Cells toward Functional Cardiomyocytes in 96-Well Microplates. Scientific Reports 2020, 10, 18498.

66. Mordwinkin, N.; Mordwinkin, N.; Burridge, P.; Burridge, P.; Wu, J.; Wu, J. A Review of Human Pluripotent Stem Cell-Derived Cardiomyocytes for High-Throughput Drug Discovery, Cardiotoxicity Screening, and Publication Standards. J. of Cardiovasc. Trans. Res 2013, 6, 22-30.

67. Kenar, H.; Kenar, H.; Kose, G.; Kose, G.; Hasirci, V.; Hasirci, V. Design of a 3D Aligned Myocardial Tissue Construct from Biodegradable Polyesters. J Mater Sci: Mater Med 2010, 21, 989-997.

68. Allen, A. C.; Barone, E.; Momtahan, N.; Crosby, C. O.; Tu, C.; Deng, W.; Polansky, K.; Zoldan, J. Temporal Impact of Substrate Anisotropy on Differentiating Cardiomyocyte Alignment and Functionality. Tissue Engineering. Part A 2019, 25, 1426-1437.

69. Ding, M.; Andersson, H.; Martinsson, S.; Sabirsh, A.; Jonebring, A.; Wang, Q.; Plowright, A. T.; Drowley, L. Aligned Nanofiber Scaffolds Improve Functionality of Cardiomyocytes Differentiated from Human Induced Pluripotent Stem Cell-Derived Cardiac Progenitor Cells. Scientific Reports 2020, 10, 13575.

70. Fleischer, S.; Shapira, A.; Regev, O.; Nseir, N.; Zussman, E.; Dvir, T. Albumin Fiber Scaffolds for Engineering Functional Cardiac Tissues. Biotechnology and Bioengineering 2014, 111, 1246-1257.

71. Han, J.; Wu, Q.; Xia, Y.; Wagner, M. B.; Xu, C. Cell Alignment Induced by Anisotropic Electrospun Fibrous Scaffolds Alone has Limited Effect on Cardiomyocyte Maturation. Stem Cell Research 2016, 16, 740-750.

72. Bedada, F. B.; Wheelwright, M.; Metzger, J. M. Maturation Status of Sarcomere Structure and Function in Human Ipsc-Derived Cardiac

Myocytes. Molecular Cell Research 2016, 1863, 1829-1838.

73. Rao, C.; Prodromakis, T.; Chaudhry, U.; Camelliti, P.; Yacoub, M. H.; Darzi, A.; Ali, N. N.; Athanasiou, T.; Terracciano, C. M. Structured Culture Scaffolds Improve the Calcium Handling Properties of Cardiomyocytes Differentiated from Induced Pluripotent Stem Cells. Biophysical Journal 2012, 102, 103a.

74. Kumar, N.; Sridharan, D.; Palaniappan, A.; Dougherty, J. A.; Czirok, A.; Isai, D. G.; Mergaye, M.; Angelos, M. G.; Powell, H. M.; Khan, M. Scalable Biomimetic Coaxial Aligned Nanofiber Cardiac Patch: A Potential Model for "Clinical Trials in a Dish". Frontiers in Bioengineering and Biotechnology 2020, 8, 567842.